# Peptidoglycan Recycling Promotes Outer Membrane Integrity and Carbapenem Tolerance in *Acinetobacter baumannii*

Nowrosh Islam,[a] Misha I. Kazi,[a] Katie N. Kang,[a] Jacob Biboy,[b] Joe Gray,[c] Feroz Ahmed,[a] Richard D. Schargel,[a] ⓘCara C. Boutte,[a] Tobias Dörr,[d,e,f] Waldemar Vollmer,[b] ⓘJoseph M. Boll[a]

[a]Department of Biology, University of Texas—Arlington, Arlington, Texas, USA
[b]Centre for Bacterial Cell Biology, Biosciences Institute, Newcastle University, Newcastle upon Tyne, United Kingdom
[c]Biosciences Institute, Newcastle University, Newcastle upon Tyne, United Kingdom
[d]Weill Institute for Cell and Molecular Biology, Cornell University, Ithaca, New York, USA
[e]Department of Microbiology, Cornell University, Ithaca, New York, USA
[f]Cornell Institute of Host-Microbe Interactions and Disease, Cornell University, Ithaca, New York, USA

Nowrosh Islam and Misha I. Kazi contributed equally. Order of first authors was determined based on alphabetical order of surname.

**ABSTRACT** $\beta$-Lactam antibiotics exploit the essentiality of the bacterial cell envelope by perturbing the peptidoglycan layer, typically resulting in rapid lysis and death. Many Gram-negative bacteria do not lyse but instead exhibit "tolerance," the ability to sustain viability in the presence of bactericidal antibiotics for extended periods. Antibiotic tolerance has been implicated in treatment failure and is a stepping-stone in the acquisition of true resistance, and the molecular factors that promote intrinsic tolerance are not well understood. *Acinetobacter baumannii* is a critical-threat nosocomial pathogen notorious for its ability to rapidly develop multidrug resistance. Carbapenem $\beta$-lactam antibiotics (i.e., meropenem) are first-line prescriptions to treat *A. baumannii* infections, but treatment failure is increasingly prevalent. Meropenem tolerance in Gram-negative pathogens is characterized by morphologically distinct populations of spheroplasts, but the impact of spheroplast formation is not fully understood. Here, we show that susceptible *A. baumannii* clinical isolates demonstrate tolerance to high-level meropenem treatment, form spheroplasts upon exposure to the antibiotic, and revert to normal growth after antibiotic removal. Using transcriptomics and genetic screens, we show that several genes associated with outer membrane integrity maintenance and efflux promote tolerance, likely by limiting entry into the periplasm. Genes associated with peptidoglycan homeostasis in the periplasm and cytoplasm also answered our screen, and their disruption compromised cell envelope barrier function. Finally, we defined the enzymatic activity of the tolerance determinants penicillin-binding protein 7 (PBP7) and ElsL (a cytoplasmic LD-carboxypeptidase). These data show that outer membrane integrity and peptidoglycan recycling are tightly linked in their contribution to *A. baumannii* meropenem tolerance.

**IMPORTANCE** Carbapenem treatment failure associated with "superbug" infections has rapidly increased in prevalence, highlighting the urgent need to develop new therapeutic strategies. Antibiotic tolerance can directly lead to treatment failure but has also been shown to promote the acquisition of true resistance within a population. While some studies have addressed mechanisms that promote tolerance, factors that underlie Gram-negative bacterial survival during carbapenem treatment are not well understood. Here, we characterized the role of peptidoglycan recycling in outer membrane integrity maintenance and meropenem tolerance in *A. baumannii*. These studies suggest that the pathogen limits antibiotic concentrations in the periplasm and highlight physiological processes that could be targeted to improve antimicrobial treatment.

**1**

The cell envelope is a dynamic barrier composed of an inner (cytoplasmic) membrane, a periplasm that includes a thin peptidoglycan (PG) layer, and an outer membrane, which is a selective barrier that restricts the entry of toxins and antibiotics. While the PG layer is known to protect against bursting due to cell turgor, the outer membrane also contributes to protection against lysis when external osmotic conditions change (1). Perturbation of the outer membrane or PG envelope layers induces lysis in many bacteria, but regulated responses that fortify the envelope can maintain envelope homeostasis to promote pathogen survival during stress exposure (2).

Antibiotic treatment failure is a growing threat to public health and has primarily been associated with antibiotic resistance (i.e., growth with antibiotic treatment). However, antibiotic tolerance, a population's ability to survive otherwise toxic levels of antibiotic treatment for extended periods, likely acts as a stepping-stone to true resistance (3–5). Antibiotic tolerance is characterized by the survival of cell populations in a nondividing state, where the MIC does not change, and cells revert to normal growth when the antibiotic is removed, degraded, or diluted (6–8). Molecular factors that extend survival during treatment increase the probability of resistance-conferring mutations or the occurrence of horizontal gene transfer (3).

Carbapenems are important $\beta$-lactam therapeutics because they possess potent broad-spectrum activity and are not susceptible to common resistance mechanisms (9, 10). In fact, meropenem is a last-line carbapenem antibiotic used to treat multidrug-resistant Gram-negative infections (11, 12). While meropenem treatment is typically reserved to fight multidrug-resistant bacteria, it is a first-line prescription against the highly drug-resistant nosocomial pathogen *Acinetobacter baumannii* (13, 14). Carbapenem-resistant *A. baumannii* has become commonplace among hospital-acquired infections. In 2019, the Centers for Disease Control and Prevention listed carbapenem-resistant *A. baumannii* as one of the most urgent threats to public health (15), and a report by the World Health Organization prioritized the pathogen as critical for new antibiotic development (16), underscoring its clinical significance.

We reasoned that since tolerance is a prerequisite for true resistance, tolerance factors may be widespread among meropenem-susceptible *A. baumannii* strains. Defining intrinsic tolerance factors in *A. baumannii* may offer fundamental insight into how resistance mechanisms rapidly spread among populations and provide new targets to combat tolerant pathogens. While our understanding of resistance mechanisms that cause antibiotic treatment failure has been well documented, tolerance factors that precede the acquisition of true resistance are limited.

Here, we show that susceptible *A. baumannii* strains, including laboratory-adapted and recent clinical isolates, survive for extended periods (>24 h) in high levels of meropenem, demonstrating widespread tolerance. Meropenem induces cell wall-deficient spheroplast formation in *A. baumannii*, as shown in other Gram-negative pathogens (17–19). After the removal of the antibiotic, cells readily revert to the canonical *A. baumannii* coccobacillus morphology and resume growth. Time-resolved transcriptome sequencing during meropenem treatment showed the differential expression of genes that coordinate a regulatory response to reduce the intracellular meropenem concentration. In addition, we found that PG recycling was also a major contributor to *A. baumannii* survival during meropenem treatment, and the disruption of genes encoding periplasmic and cytoplasmic PG maintenance enzymes compromises outer membrane integrity. Finally, we also define the enzymatic activities of two novel tolerance determinants, penicillin-binding protein 7 (PBP7) (encoded by *pbpG*) and ElsL (also known as LdtK [20]). Together, these studies show that *A. baumannii* coordinates several pathways to limit meropenem-induced cell envelope damage. These findings provide new targets to direct antimicrobial therapies that optimize the effective treatment of *A. baumannii* and prevent the spread of resistance.

## RESULTS

**Meropenem-susceptible *A. baumannii* strains are tolerant, form spheroplasts, and resume normal morphology and growth upon removal of the bactericidal antibiotic.** Previous work showed that *Vibrio cholerae* (17, 18), *Pseudomonas aeruginosa* (19), and pathogens of the *Enterobacterales* order (21, 22) form viable, nondividing spheroplasts when exposed to lethal concentrations of $\beta$-lactam antibiotics over several hours. Importantly, spheroplasts revert to normal rod-shaped growth when the antibiotic concentration is sufficiently reduced (21), demonstrating a short-term survival mechanism that directly contributes to antibiotic treatment failure.

To determine if populations of *A. baumannii* strains can tolerate meropenem treatment over time, stationary-phase cultures from susceptible *A. baumannii* isolates, including recent clinical isolates, were treated with high levels (10 $\mu$g/mL; 62.5-fold the MIC for strain ATCC 17978) of the antibiotic. Treated cultures demonstrated only a slight decrease in viability after 24 h, relative to untreated cultures (Fig. 1A; see also Fig. S1A in the supplemental material). In contrast, meropenem treatment of cells in the logarithmic growth phase caused rapid lysis (Fig. S1B). Therefore, *A. baumannii* strains are highly tolerant to normally lethal meropenem concentrations during slow growth, a relevant physiological state during infection when the cell is known to fortify the cell envelope (23). While these data agree with the current dogma that $\beta$-lactam-dependent killing is strictly proportional to the growth rate (7, 24, 25), subsequent analysis revealed that stationary-phase *A. baumannii* cells experience significant cell envelope damage upon meropenem treatment. After 12 h, stationary-phase cells treated with meropenem demonstrated notable morphological changes relative to untreated cells (Fig. 1B; Fig. S2). All strains showed measurable increases in the surface area and width of treated cells relative to untreated cells (Fig. 1C; Fig. S2). To visualize changes in PG assembly, cells were treated with a fluorescent derivative of D-alanine [NBD-(linezolid-7-nitrobenz-2-oxa-1,3-diazol-4-yl)-amino-D-alanine (NADA)], which is incorporated into the peptidoglycan by PBPs and LD-transpeptidases (26–29). A significant decrease in the NADA intensity was evident in meropenem-treated cultures relative to untreated cultures at 12 h (Fig. 1B and D; Fig. S2), suggesting the degradation of the cell wall and spheroplast formation, as previously shown in other $\beta$-lactam-tolerant Gram-negative bacteria (17, 21). Thus, tolerance in stationary phase is not just a simple function of growth inhibition but rather is an active response to significant cell envelope damage in *A. baumannii*.

Since meropenem-treated *A. baumannii* spheroplasts were viable after plating (Fig. 1A; Fig. S1A), we also wanted to determine if the characteristic *A. baumannii* coccobacillus morphology was restored after antibiotic removal. Cells treated with meropenem for 12 h were washed and grown in fresh medium without the antibiotic. At 12 h posttreatment, no spheroplasts were found after antibiotic removal (Fig. 1E), and wild-type (WT) morphology was largely restored (Fig. 1F), suggesting that PG was being synthesized and remodeled (Fig. 1E). We also tracked the cell wall content during meropenem exposure and subsequent recovery. Fluorescence intensity measurements showed a stepwise decrease in the fluorescence intensity 6 and 12 h after treatment relative to the start of the experiment (0 h) (Fig. 1G), confirming PG degradation during meropenem treatment. After 12 h of meropenem treatment, cells were washed to remove the antibiotic, resuspended in fresh medium, and again stained with NADA. Fluorescence intensity measurements 12 h after meropenem treatment showed a drastic increase in NADA incorporation (Fig. 1G), suggesting that the cell resumed PG remodeling and synthesis. Furthermore, the fluorescence intensity appeared higher at the midcell of some cells (Fig. 1E, white arrows), suggesting that the recovered population had resumed division. Together, these data support a model where *A. baumannii* spheroplasts revert to wild-type morphology and growth when meropenem treatment is stopped.

**Transcriptome analysis highlights differentially regulated pathways with a putative role in *A. baumannii* tolerance.** Many Gram-negative pathogens rapidly form tolerant spheroplasts during meropenem exposure (17, 21); however, *A. baumannii* spheroplast formation is delayed. We first observed spheroplast formation only after
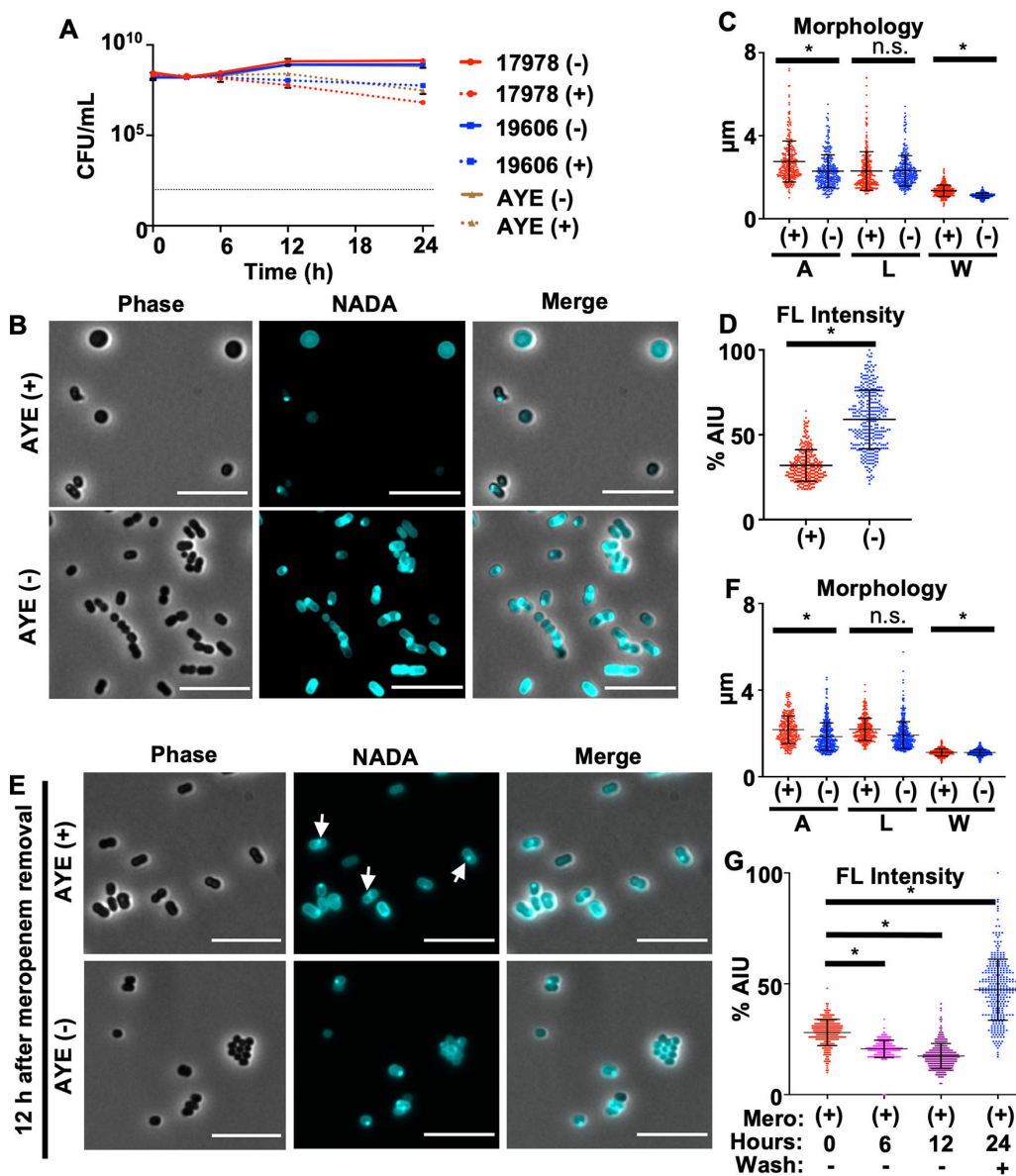
FIG 1 *Acinetobacter baumannii* strains are tolerant to meropenem. (A) CFU of *A. baumannii* strains ATCC 17978, ATCC 19606, and AYE untreated (−) or treated (+) with meropenem over 24 h. Each killing assay was independently replicated three times, and one representative data set is reported. Error bars indicate standard deviations (SD) from the means. The dotted black line indicates the level of detection. (B) Phase-contrast and fluorescence microscopy of treated or untreated *A. baumannii* strain AYE after 12 h. Bars, 10 $\mu$m. (C) Area (A), length (L), and width (W) quantitations of cells in panel B ($n = 300$). (D) Fluorescence (FL) signal intensity quantitation in percent arbitrary intensity units (AIU) of treated versus untreated cells in panel B ($n = 300$). (E) After 12 h of meropenem treatment, the antibiotic was removed, and cells were resuspended in fresh medium without the antibiotic and stained with NADA. Cells were imaged after a 12-h recovery period and showed that the characteristic coccobacillus morphology was restored. White arrows indicate fluorescence intensity at the midcell. (F) Area, length, and width (W) of cells in panel E ($n = 300$). (G) Fluorescence signal intensity in percent AIU for treated versus untreated cells ($n = 300$) at 0, 6, and 12 h during meropenem treatment and 12 h after the removal of the antibiotic. Significance was determined using an unpaired *t* test ($P < 0.05$) in treated versus untreated cells. An asterisk indicates significant differences between treated and untreated cells. n.s., not significant. Error bars indicate SD from the means.

8 h, with large numbers within the population accumulating by 12 h (Fig. 1B and C; Fig. S2). To define transcriptional alterations associated with spheroplast-associated tolerance, we isolated RNA from treated and untreated cells at 0.5, 3, and 9 h. While subtle changes in gene expression were evident at 0.5 and 3 h, differential expression patterns were more obvious at 9 h in treated cultures relative to untreated cultures
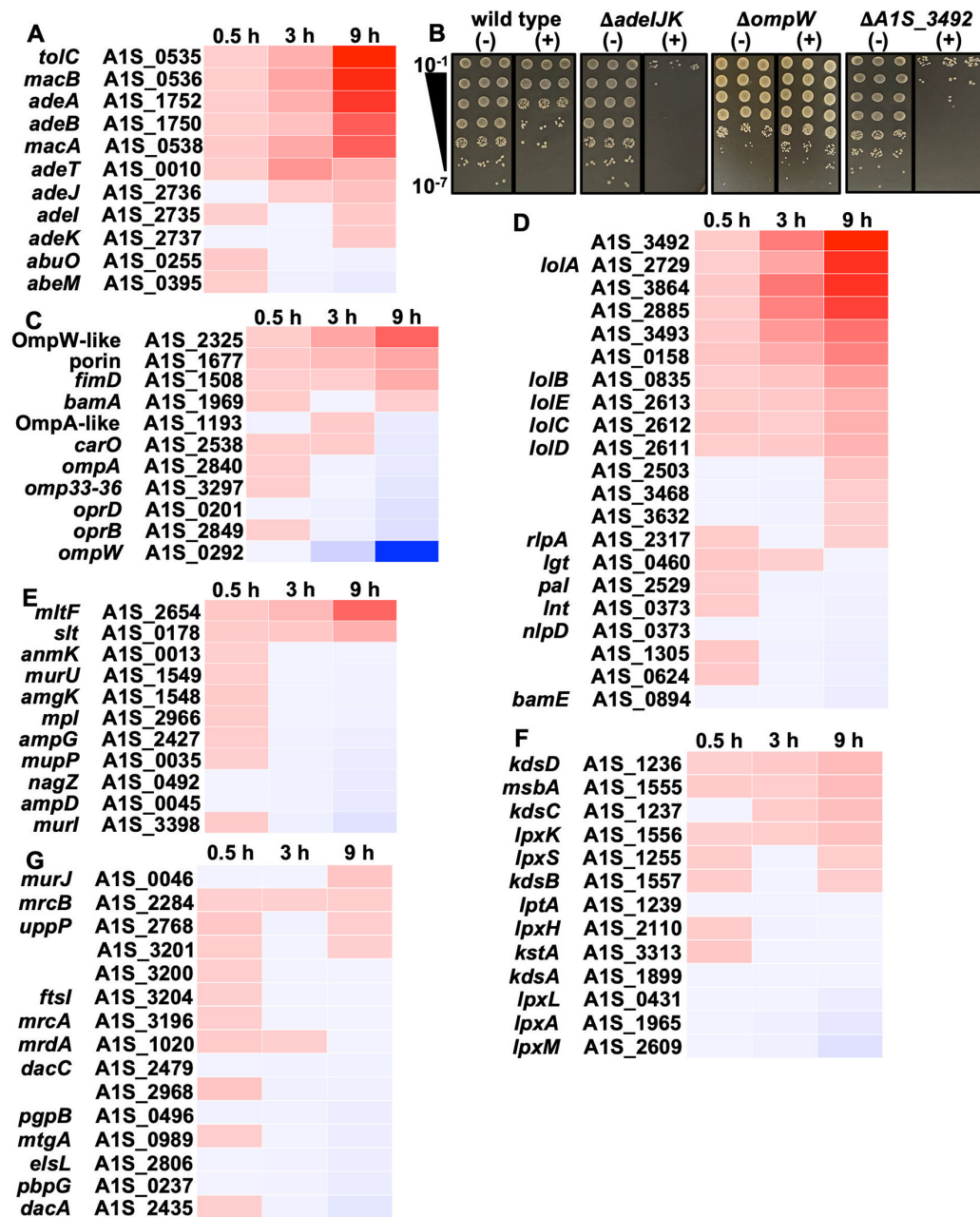
**A**

|  |  | 0.5 h | 3 h | 9 h |
|---|---|---|---|---|
| *tolC* | A1S_0535 |  |  |  |
| *macB* | A1S_0536 |  |  |  |
| *adeA* | A1S_1752 |  |  |  |
| *adeB* | A1S_1750 |  |  |  |
| *macA* | A1S_0538 |  |  |  |
| *adeT* | A1S_0010 |  |  |  |
| *adeJ* | A1S_2736 |  |  |  |
| *adeI* | A1S_2735 |  |  |  |
| *adeK* | A1S_2737 |  |  |  |
| *abuO* | A1S_0255 |  |  |  |
| *abeM* | A1S_0395 |  |  |  |

**B**

wild type   ΔadeIJK   ΔompW   ΔA1S_3492
(−) (+)   (−) (+)   (−) (+)   (−) (+)

$10^{-1}$
$10^{-7}$

**C**

|  |  | 0.5 h | 3 h | 9 h |
|---|---|---|---|---|
| OmpW-like | A1S_2325 |  |  |  |
| porin | A1S_1677 |  |  |  |
| *fimD* | A1S_1508 |  |  |  |
| *bamA* | A1S_1969 |  |  |  |
| OmpA-like | A1S_1193 |  |  |  |
| *carO* | A1S_2538 |  |  |  |
| *ompA* | A1S_2840 |  |  |  |
| *omp33-36* | A1S_3297 |  |  |  |
| *oprD* | A1S_0201 |  |  |  |
| *oprB* | A1S_2849 |  |  |  |
| *ompW* | A1S_0292 |  |  |  |

**D**

|  |  | 0.5 h | 3 h | 9 h |
|---|---|---|---|---|
|  | A1S_3492 |  |  |  |
| *lolA* | A1S_2729 |  |  |  |
|  | A1S_3864 |  |  |  |
|  | A1S_2885 |  |  |  |
|  | A1S_3493 |  |  |  |
|  | A1S_0158 |  |  |  |
| *lolB* | A1S_0835 |  |  |  |
| *lolE* | A1S_2613 |  |  |  |
| *lolC* | A1S_2612 |  |  |  |
| *lolD* | A1S_2611 |  |  |  |
|  | A1S_2503 |  |  |  |
|  | A1S_3468 |  |  |  |
|  | A1S_3632 |  |  |  |
| *rlpA* | A1S_2317 |  |  |  |
| *lgt* | A1S_0460 |  |  |  |
| *pal* | A1S_2529 |  |  |  |
| *lnt* | A1S_0373 |  |  |  |
| *nlpD* | A1S_0373 |  |  |  |
|  | A1S_1305 |  |  |  |
|  | A1S_0624 |  |  |  |
| *bamE* | A1S_0894 |  |  |  |

**E**

|  |  | 0.5 h | 3 h | 9 h |
|---|---|---|---|---|
| *mltF* | A1S_2654 |  |  |  |
| *slt* | A1S_0178 |  |  |  |
| *anmK* | A1S_0013 |  |  |  |
| *murU* | A1S_1549 |  |  |  |
| *amgK* | A1S_1548 |  |  |  |
| *mpl* | A1S_2966 |  |  |  |
| *ampG* | A1S_2427 |  |  |  |
| *mupP* | A1S_0035 |  |  |  |
| *nagZ* | A1S_0492 |  |  |  |
| *ampD* | A1S_0045 |  |  |  |
| *murI* | A1S_3398 |  |  |  |

**F**

|  |  | 0.5 h | 3 h | 9 h |
|---|---|---|---|---|
| *kdsD* | A1S_1236 |  |  |  |
| *msbA* | A1S_1555 |  |  |  |
| *kdsC* | A1S_1237 |  |  |  |
| *lpxK* | A1S_1556 |  |  |  |
| *lpxS* | A1S_1255 |  |  |  |
| *kdsB* | A1S_1557 |  |  |  |
| *lptA* | A1S_1239 |  |  |  |
| *lpxH* | A1S_2110 |  |  |  |
| *kstA* | A1S_3313 |  |  |  |
| *kdsA* | A1S_1899 |  |  |  |
| *lpxL* | A1S_0431 |  |  |  |
| *lpxA* | A1S_1965 |  |  |  |
| *lpxM* | A1S_2609 |  |  |  |

**G**

|  |  | 0.5 h | 3 h | 9 h |
|---|---|---|---|---|
| *murJ* | A1S_0046 |  |  |  |
| *mrcB* | A1S_2284 |  |  |  |
| *uppP* | A1S_2768 |  |  |  |
|  | A1S_3201 |  |  |  |
|  | A1S_3200 |  |  |  |
| *ftsI* | A1S_3204 |  |  |  |
| *mrcA* | A1S_3196 |  |  |  |
| *mrdA* | A1S_1020 |  |  |  |
| *dacC* | A1S_2479 |  |  |  |
|  | A1S_2968 |  |  |  |
| *pgpB* | A1S_0496 |  |  |  |
| *mtgA* | A1S_0989 |  |  |  |
| *elsL* | A1S_2806 |  |  |  |
| *pbpG* | A1S_0237 |  |  |  |
| *dacA* | A1S_2435 |  |  |  |

**FIG 2** Differentially regulated genes in response to meropenem treatment in *A. baumannii*. Heat maps show the fold changes in genes expressed at 0.5, 3, and 9 h of meropenem treatment relative to wild-type ATCC 17978 ($P < 0.05$). (A) Differentially regulated genes associated with efflux. (B) Dilution spot assays (in triplicate) of wild-type, Δ*adeIJK*, Δ*ompW*, and Δ*A1S_3492* strains with (+) or without (−) meropenem treatment. (C to G) Same as panel A but with pathway analysis including genes associated with outer membrane porins (C), outer membrane lipoproteins and their transporters (D), PG recycling (E), LOS biosynthesis (F), and PG biosynthesis (G).

(Fig. 2). Genes associated with efflux were increasingly upregulated with each time point (Fig. 2A), suggesting that the cell quickly and continually responds to meropenem treatment by actively expelling the toxic compound. Upregulated efflux genes included *adeAB*, *adeIJK*, and *macAB-tolC*, all of which have been implicated in antibiotic efflux (30–32); specifically, β-lactam efflux is associated with the AdeIJK RND-type pump (33, 34). To validate the role of AdeIJK in meropenem tolerance or resistance, we constructed a genetic knockout (Δ*adeIJK*), which was subjected to high-level meropenem treatment (Fig. 2B). At 24 h posttreatment, the Δ*adeIJK* mutant was more than

1,000-fold more susceptible to meropenem-mediated killing than the wild type, showing that efflux contributes to tolerance.

Porins represent the major entryway for carbapenems such as meropenem to enter the periplasm (35), where they inhibit transpeptidation to cross-link the stem peptides of adjacent PG strands. Decreased expression of many porin-associated genes was evident in treated cultures relative to untreated cultures (Fig. 2C), suggesting that the cell also limits meropenem entry by reducing porin gene expression in response to treatment. However, the temporal expression of porin-associated genes was delayed relative to efflux, in general. For example, the porin genes *carO* and *oprD* were downregulated at later time points only (Fig. 2C). The deletion of *carO* is associated with carbapenem resistance in *A. baumannii* (36), and it was found to be an influx channel for carbapenems (37), while OprD has also been associated with clinical carbapenem resistance in *A. baumannii* (38), suggesting that reduced expression may strategically limit meropenem entry. Interestingly, the largest reduction in gene expression was associated with *ompW*, which encodes a predicted β-barrel protein (OmpW) that supports iron uptake (39), but our understanding of its biological function or how it contributes to carbapenem resistance or tolerance is limited. Notably, in *Vibrio cholerae*, decreased iron uptake regulated by the VxrAB two-component system promotes spheroplast recovery by reducing oxidative stress during β-lactam treatment (40, 41), potentially suggesting a similar iron reduction role for the downregulation of *ompW*. To further validate the RNA sequencing data set, we analyzed the Δ*ompW* mutant in a meropenem killing assay, which showed an ~10-fold increase in survival relative to the wild type (Fig. 2B). Thus, the downregulation of *ompW* contributes to tolerance.

Consistent with previously reported *A. baumannii* transcriptional data sets under stress conditions (42–44), meropenem treatment also induces the expression of genes encoding putative outer membrane lipoproteins and their transporters (LolA to -D) (Fig. 2D). Outer membrane lipoproteins fortify the *Escherichia coli* cell envelope by providing structural rigidity, where some outer membrane lipoproteins are covalently attached to the underlying PG network (1, 45). Finally, we made an isogenic mutant of *A1S_3492*, encoding a putative outer membrane lipoprotein that was strongly upregulated following meropenem exposure. The Δ*A1S_3492* mutant showed an ~100-fold increase in meropenem susceptibility relative to the wild type (Fig. 2B). Together, the analyses of efflux, porin, and lipoprotein mutants suggest a transcriptional response that protects *A. baumannii* from meropenem-dependent killing during treatment.

The transcription of genes associated with PG remodeling was only slightly altered, with the notable exception of two genes encoding putative lytic transglycosylases, including the outer membrane-bound protein MltF and a soluble protein, Slt, both of which were upregulated (Fig. 2E). Lytic transglycosylases were recently shown to fulfill an important role in clearing un-cross-linked or mis-cross-linked periplasmic muropeptide fragments, which can accumulate to detrimental levels in the presence of β-lactams, potentially explaining the adaptive value of their upregulation (46, 47). Finally, genes involved in lipooligosaccharide (LOS) and PG biosynthesis were slightly altered (Fig. 2F and G).

**Genes and pathways that contribute to *A. baumannii* fitness during meropenem treatment.** While transcriptome sequencing analyses offer insight into specific stress responses, one limitation is that differentially regulated genes often do not impact fitness due to redundancy or pleiotropic effects. Therefore, we also performed transposon sequencing (Tn-seq) on *A. baumannii* strain ATCC 17978. Using previously constructed high-density transposon libraries generated in wild-type *A. baumannii* (20, 48), stationary-phase cultures were either treated with meropenem or left untreated during incubation at 37°C. After 6, 9, and 12 h, cells were collected, insertions were mapped, and comparisons between treated and untreated cultures were used to identify meropenem tolerance factors. The screen was answered by several novel factors, some of which are the subject of a separate study, but also revealed the importance of outer membrane integrity and PG maintenance (Fig. 3A). To validate our screen, we assessed survival in the presence and absence of meropenem in several mutants, including Δ*ompA*, Δ*lpxM*,
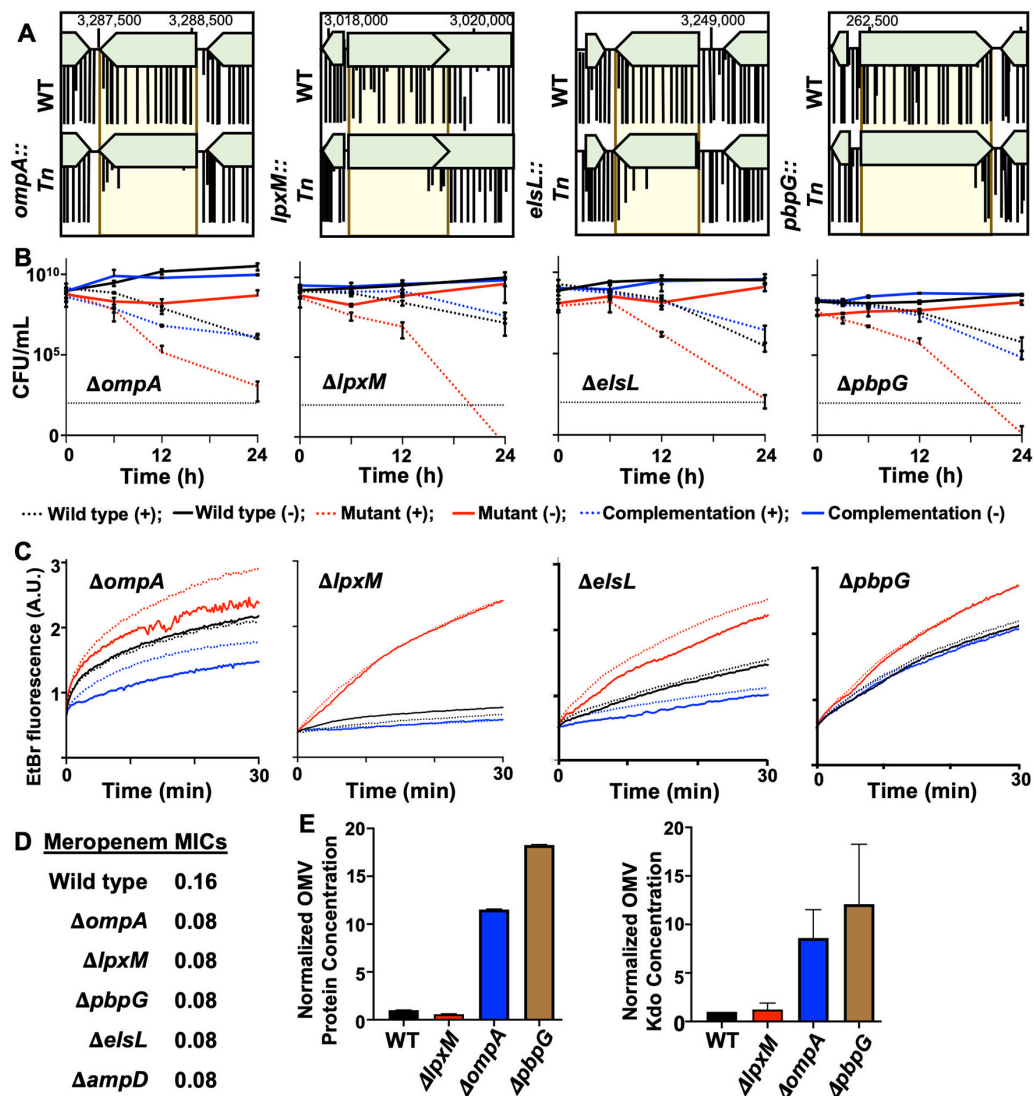
**FIG 3** Genes encoding outer membrane integrity and PG maintenance contribute to meropenem tolerance in *A. baumannii*. (A) Tn-seq analysis of genes required for meropenem tolerance at 12 h. (B) Survival in isogenic mutants was calculated as CFU per milliliter over 24 h during meropenem treatment. Data were collected from two experiments in triplicate. Error bars represent the averages from 3 technical replicates ± SD. (C) Permeability assays using ethidium bromide (EtBr) over 0.5 h. A.U., arbitrary units. Lines depict the means from three technical replicates. (D) MICs of wild-type and isogenic *A. baumannii* mutant strains. (E) Relative quantification of protein (left) and Kdo (right) concentrations of outer membrane vesicles (OMVs) in wild-type (WT) and mutant strains. Each experiment was independently replicated three times, and one representative data set is reported. Error bars indicate SD from the means. An asterisk indicates significant differences relative to the WT strain ($P < 0.05$).

Δ*pbpG*, and Δ*elsL* (also known as *ldtK* [20]) (Fig. 3B). All mutants showed at least a 2- to 3-log fold reduction in viable counts relative to the wild type at 12 h and a >5-log fold reduction at 24 h. Importantly, the meropenem MICs did not change significantly in the mutants relative to the wild type (Fig. 3D). These studies suggest that *A. baumannii* fitness during meropenem treatment is dependent on outer membrane integrity and PG maintenance factors.

OmpA is a highly conserved monomeric β-barrel protein with a periplasmic domain that noncovalently attaches the outer membrane to the PG network (49). It is highly abundant in *A. baumannii* (50) and coordinates with efflux pumps to export antibacterial compounds from the periplasm (51, 52). OmpA is also known to stabilize the outer membrane; *ompA* deletion/disruption induces outer membrane vesicle formation and increases permeability (53). To test the hypothesis that *ompA* deletion perturbs the

outer membrane to promote meropenem entry in *A. baumannii*, we performed two assays, including permeability measurements (Fig. 3C) and outer membrane vesiculation assays (Fig. 3E). Relative to the wild type, the Δ*ompA* mutant exhibited increased outer membrane vesicle formation and permeability to ethidium bromide (EtBr), which is similar in size to meropenem. We also measured ethidium bromide influx in the Δ*lpxM*, Δ*pbpG*, and Δ*elsL* mutants (Fig. 3C). Like the Δ*ompA* mutant, all isogenic mutants had increased permeability relative to the wild type and the respective complementation strains, which restored the permeability defect. Permeability was notably reduced beyond the wild type in Δ*ompA* and Δ*elsL* complementation strains, which was likely due to protein overexpression (Fig. S3A and B). Furthermore, meropenem treatment did not exacerbate permeability in the wild type or any of the mutants (Fig. 3C), suggesting that it does not directly destabilize outer membrane barrier function. Since we previously reported that the Δ*elsL* mutant produces excess outer membrane vesicles (20), and all of the mutants showed increased permeability, we also tested vesicle formation in the Δ*lpxM* and Δ*pbpG* mutants (Fig. 3E). Unexpectedly, the Δ*pbpG* mutant produced excess outer membrane vesicles relative to the wild type and all other mutants. In contrast, the Δ*lpxM* mutant did not.

Interestingly, the Δ*lpxM* mutant was the only strain that showed increased permeability but not hypervesiculation. LpxM catalyzes the transfer of two lauroyl ($C_{12:0}$) groups from an acyl carrier protein to the *R*-3′- and *R*-2-hydroxymyristate positions of lipid A during LOS biosynthesis (54). Mutations that reduce LOS acylation are known to increase the fluidity of the lipid bilayer and could also impact the folding/function of outer membrane porins (55, 56). Either or both of these mechanisms could increase the entry of meropenem into the periplasmic space or disrupt efflux mechanisms that actively pump the compound out of the cell.

We also characterized the morphology of each mutant during growth (Fig. S3C to F). We found that relative to the wild type, Δ*ompA* cells were chained, and NADA incorporation was reduced (Fig. S3C), suggesting that OmpA is required for the proper function of PG enzymes (division proteins and LD/DD-transpeptidases that incorporate NADA and/or increase carboxypeptidase activity). Δ*lpxM* and Δ*pbpG* mutants showed increased NADA incorporation (Fig. S3D and E), which is consistent with increased outer membrane permeability (or decreased carboxypeptidase activity). Δ*pbpG* cells were also clumped (Fig. S3E), suggesting that the cells could not properly separate during division. As previously reported (20), the Δ*elsL* mutant exhibited cell rounding (Fig. S3F).

**PBP7 is a DD-carboxypeptidase and -endopeptidase that catalyzes the formation of tetrapeptides.** We were intrigued by the genetic links of tolerance to PG maintenance (i.e., *pbpG* and *elsL*). Mutation of *pbpG* and *elsL* impacted outer membrane integrity (Fig. 3), but we sought to more precisely define their physiological role to determine specific pathways that contribute to meropenem tolerance. To define the activity of *A. baumannii* PBP7 (encoded by *pbpG*), *in vivo*, we isolated PG from exponential- and stationary-phase cultures of wild-type and Δ*pbpG* strains (Fig. 4A and B; Table S1). Muropeptides were generated by treatment with muramidase and separated by high-performance liquid chromatography (HPLC), and uncharacterized peaks were analyzed by tandem mass spectrometry (MS/MS) (Fig. S4), as done previously (20, 42, 57). The PG composition of the Δ*pbpG* mutant during exponential growth displayed an accumulation of two muropeptide peaks that were not present in the wild type (Fig. 4A; Table S1). MS analysis identified these peaks as disaccharide pentapeptide (Penta) (neutral mass, 1,012.19 atomic mass units [amu]; theoretical mass, 1,012.45 amu) and bis-disaccharide tetrapentapeptide (TetraPenta) (neutral mass, 1,935.60 amu; theoretical mass, 1,935.84 amu) (Fig. S4). This PG architecture suggests that these enriched muropeptide pools represent PBP7 substrates during growth. Δ*pbpG* PG during stasis exhibited a reduction in D-amino-acid-modified muropeptide pools, including TetraTri-D-Lys and TetraTri-D-Arg, and reduced 3-3 cross-link formation (Fig. 4B and C; Table S1). This is consistent with PBP7 exhibiting DD-carboxypeptidase activity, providing the abundant tetrapeptide substrate (20, 42, 57) required for LD-transpeptidases. The periplasmic LD-transpeptidase LdtJ transfers
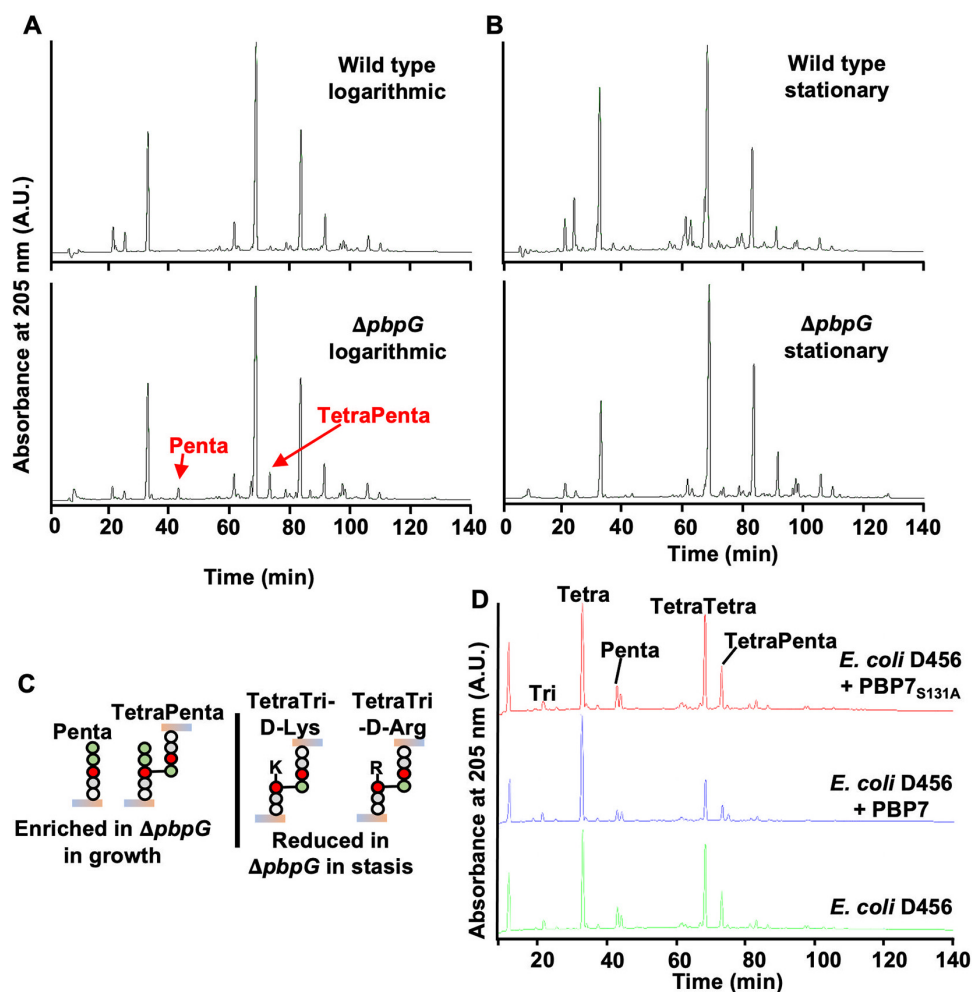
**FIG 4** PBP7 is active against pentapeptides and DD-cross-links. (A) PG isolated from wild-type and Δ*pbpG* strains in the growth phase was analyzed by HPLC. The muropeptides Penta and TetraPenta were enriched in the Δ*pbpG* mutant. (B) PG isolated from wild-type and Δ*pbpG* strains in stationary phase was analyzed by HPLC. TetraTri-D-Lys and TetraTri-D-Arg were depleted in the Δ*pbpG* mutant relative to the wild type. (C) Muropeptide structures are illustrated and were confirmed using MS/MS. (D) Recombinant PBP7 or the active-site mutant PBP7$_{S131A}$ was incubated with PG isolated from *E. coli* D456, which contains Tetra, Penta, TetraTetra, and TetraPenta as the main muropeptides. PBP7 was active against pentapeptides (DD-carboxypeptidase) and cross-linked muropeptides (DD-edopeptidase).

D-amino acid to tetrapeptides and forms 3-3 cross-links (20). Therefore, it is likely that PBP7 provides at least some of the periplasmic substrates for LdtJ-dependent transpeptidase activity during stasis.

We next tested the *in vitro* enzymatic activity. We purified recombinant PBP7 (Fig. S5A) and a predicted catalytically inactive version in which alanine replaces the active-site serine (PBP7$_{S131A}$). Purified proteins were incubated with PG from the *E. coli* strain D456 (Fig. 4D), a strain enriched in pentapeptide abundance (58), and analyzed as previously described (59). PBP7 was active against penta-, tetratetra-, and tetrapentapeptides, where each muropeptide was trimmed to the tetrapeptide form relative to the no-enzyme control. In addition, PBP7 efficiently cleaved tetrapeptide dimers into their monomers, demonstrating DD-endopeptidase activity. As expected, PBP7$_{S131A}$ did not show activity against any muropeptides. Together, these studies suggest that PBP7 has both carboxypeptidase and endopeptidase activities and that both activities enrich the periplasmic pool of monomeric tetrapeptides.

**ElsL is a cytoplasmic LD-carboxypeptidase active against tetrapeptides for PG recycling.** During β-lactam treatment, autolysins (i.e., lytic transglycosylases) are activated (7, 60), which increases the amount of PG turnover products with 1,6-anhydro-*N*-Acetylmuramic acid (Mur*N*Ac) residues. In *A. baumannii*, genes encoding the autolysins

MltF and Slt were upregulated during meropenem treatment (Fig. 2E), which likely increases the periplasmic concentrations of TetraAnh for cytoplasmic import. In *E. coli*, TetraAnh is the substrate for the LD-carboxypeptidase LdcA, which trims tetrapeptides to tripeptides (61) that are catabolized by the conserved muramidase NagZ (62, 63) and the amidase AmpD (64, 65) to generate 1,6-anhydro-Mur*N*Ac-tripeptide and free tripeptides; the latter can be further broken down into individual amino acids and used as nutrients. Furthermore, Mpl (66) can attach tripeptides to UDP-Mur*N*Ac to form UDP-Mur*N*Ac-tripeptide, an intermediate in the *de novo* PG biosynthesis pathway. However, no apparent LD-carboxypeptidase orthologue of LdcA is encoded by *A. baumannii*.

While this study was in progress, two other groups reported a characterization of ElsL as a cytoplasmic LD-carboxypeptidase (67, 68). Our results here support this conclusion. We confirmed the cytoplasmic localization of ElsL with a specific antibody that detects the native protein (Fig. 5A). After fractionation of the subcellular compartments, we were able to detect ElsL only in the cytoplasmic fraction during growth and stasis, showing that it is not exported to the periplasm.

Since ElsL is cytoplasmic, we sought to determine if it was active on tetra- and/or pentapeptide substrates. We purified recombinant ElsL and the active-site mutant ElsL$_{C138S}$ (Fig. S5B). Both enzymes were incubated with muropeptides obtained from tetrapeptide-rich PG from *E. coli* BW25113 or pentapeptide-rich PG from *E. coli* CS703-1 (59) (Fig. 5B). ElsL showed activity against tetrapeptides but not pentapeptides. The muropeptide profile revealed the formation of disaccharide tripeptide and bis-disaccharide tetratripeptide, demonstrating that ElsL cleaves the bond between the L-center of *meso*-diaminopimelic acid (*m*DAP) and the terminal D-Ala in tetrapeptides, confirming LD-carboxypeptidase activity as part of the cytoplasmic PG recycling pathway.

To further confirm that the cytoplasmic PG pathway contributes to meropenem tolerance in *A. baumannii*, we made an isogenic mutant of *ampD*, which encodes *N*-acetylmuramyl-L-alanine amidase that releases the tripeptide from anhMur*N*Ac (65). Importantly, *ampD* transposon insertions were also depleted in the meropenem tolerance screen (Fig. 5C). Like the Δ*pbpG* and Δ*elsL* mutants, the Δ*ampD* mutant was also rapidly killed when treated with meropenem relative to the wild type and the respective complementation strains (Fig. 5D). Together, these studies strongly suggest that the PG recycling pathway contributes to meropenem tolerance in *A. baumannii*. Furthermore, the formation of cytoplasmic tripeptides or tetrapeptides appears to contribute to meropenem tolerance. Combinatorial therapies that inhibit enzymes in both PG biosynthesis and recycling could provide an alternative treatment strategy.

## DISCUSSION

Many susceptible Gram-negative pathogens tolerate treatment with bactericidal antibiotics such as carbapenem β-lactams, but the molecular factors that underlie cell survival are not understood. Here, we show that meropenem treatment induces spheroplast formation in *A. baumannii* during treatment in stationary phase and that cell growth resumes upon the removal of the antibiotic. Transcriptome sequencing analysis suggested that *A. baumannii* responds to meropenem treatment by fortifying the structural integrity of the cell envelope through increased outer membrane lipoprotein and transporter gene expression. Intriguingly, autolysins were also induced, which likely contribute to tolerance via the removal of detrimental cell wall breakdown products or through their role in initiating PG recycling. Alternatively, autolysins might contribute to cell integrity by producing the necessary precursors for the formation of β-lactam-resistant 3-3 cross-links. Meropenem-treated cells also appear to limit high periplasmic accumulation of the antibiotic through the induced expression of efflux-associated genes and the downregulation of porin genes, both of which reduce periplasmic meropenem concentrations by actively pumping the antibiotic out of the cell and limiting entry, respectively.

A separate genetic (transposon) screen to identify fitness determinants revealed factors required for high-level meropenem tolerance and included genes that contribute to
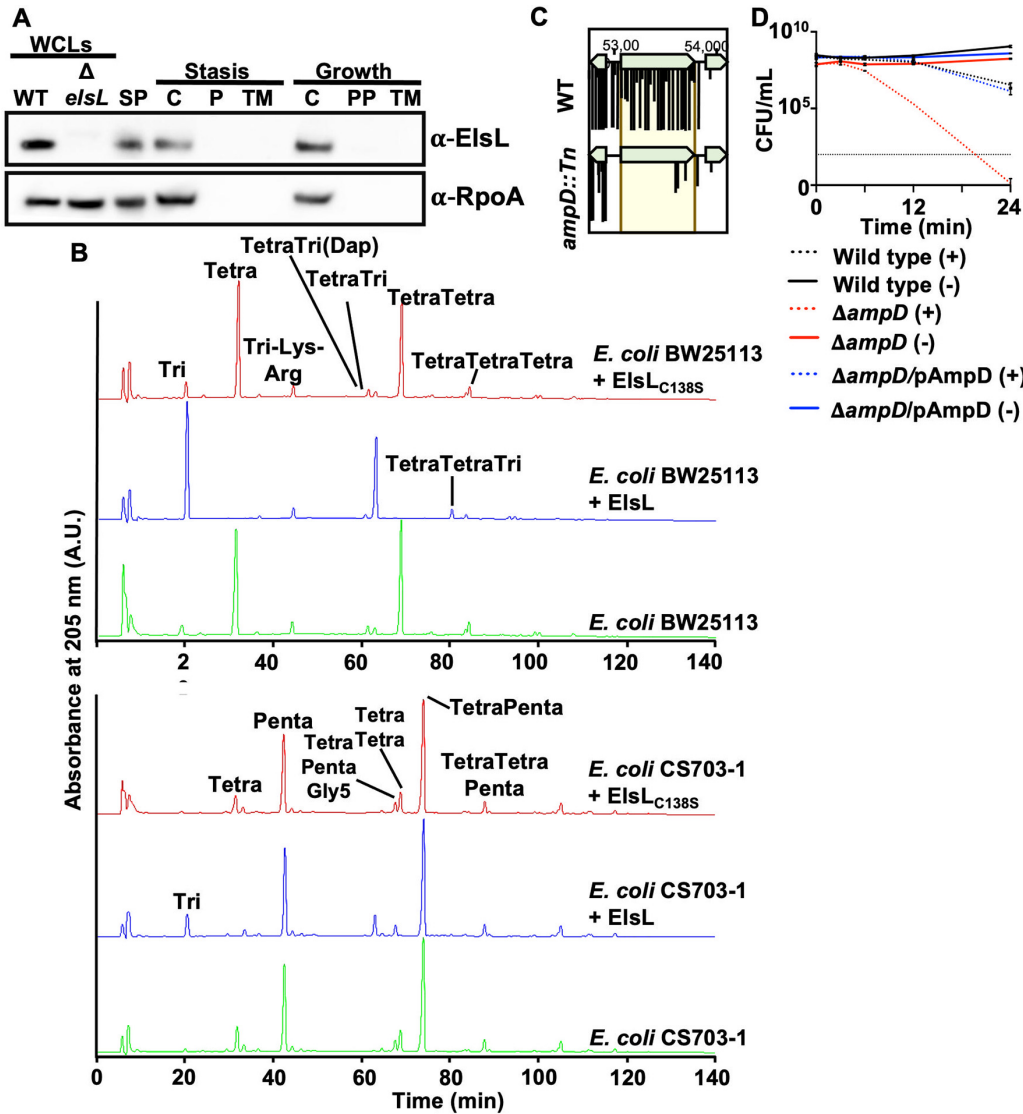
**FIG 5** ElsL is active against tetrapeptides in Tetra and TetraTetra. (A) Western blot analysis with anti-ElsL and anti-RpoA antisera. ElsL is 18.97 kDa, while RpoA is 37.27 kDa. WCLs, whole-cell lysates; SP, spheroplast; C, cytoplasm; PP, periplasm; TM, total membrane fraction. (B) Recombinant ElsL or the active-site mutant ElsL$_{C135}$ was incubated with PG isolated from *E. coli* strain BW25113 (tetrapeptide rich) (top) or strain CS703-1 (pentapeptide rich) (bottom). ElsL was active against tetrapeptides but not pentapeptides. (C) Tn-seq analysis of *ampD*::Tn insertions relative to the wild type 12 h after meropenem treatment. (D) Meropenem tolerance assay in the Δ*ampD* mutant, which encodes a well-conserved cytoplasmic enzyme required for PG recycling. Error bars represent the averages from 3 technical replicates ± SD from the means.

outer membrane permeability (*lpxM*, *ompA*, *pbpG*, and *elsL*) and cell envelope stability (*ompA*, *pbpG*, and *elsL*). Furthermore, genes in the cytoplasmic PG recycling pathway, *elsL* and *ampD*, also answered the screen. Together, the data from transcriptomics and genetic screens suggested that factors working to maintain cell envelope homeostasis through integrity maintenance of the outer membrane and PG network contribute to meropenem tolerance in *A. baumannii* (Fig. 6).

While we showed that several tolerance factors are transcriptionally regulated, we do not know which transcriptional regulators control these responses. A previous study found that PhoPQ-dependent outer membrane modifications promoted survival in cell wall-deficient spheroplasts (22), presumably by fortifying the outer membrane to counter large loads of turgor pressure typically absorbed by the cell wall. Specifically, PhoPQ was activated in response to meropenem treatment. *A. baumannii* does not
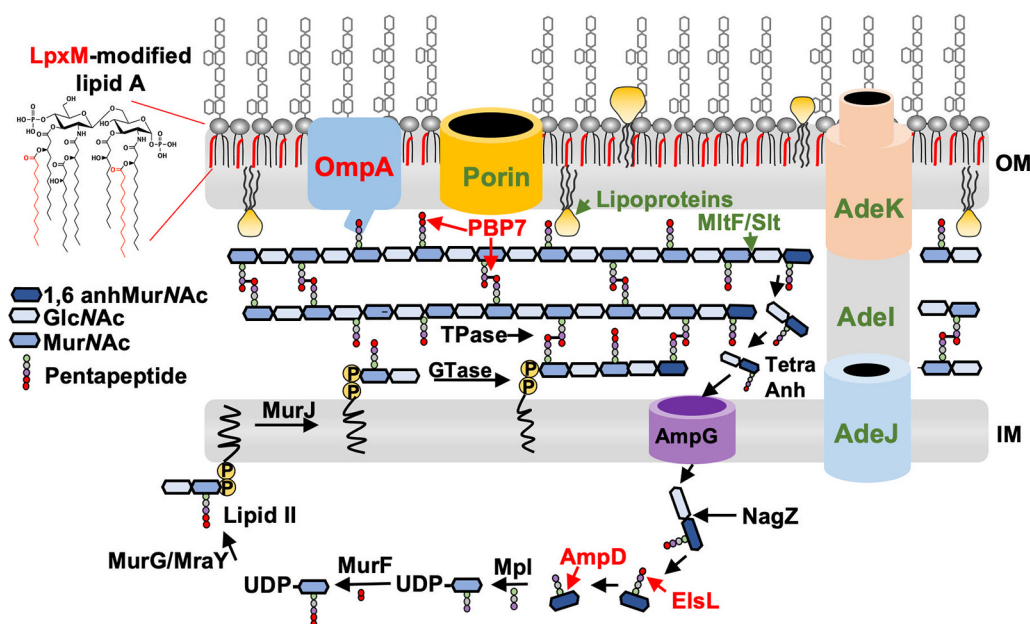
**FIG 6** Model showing mechanisms that promote meropenem tolerance in *A. baumannii*. Based on transcriptomic analysis, several genes are differentially expressed after treatment with high levels of meropenem. Pathways include the upregulation of the AdeIJK efflux pump, lipoproteins, and the MltF/Slt autolysins, while porins, including CarO and OprD, were downregulated (green). Fitness screens showed that several genes involved in the outer membrane (OM), periplasmic, and cytoplasmic pathways promote meropenem tolerance. Pathways include OmpA, which tethers the outer membrane to the peptidoglycan; LpxM, which increases hydrophobic packing in the outer membrane; the DD-carboxypeptidase and DD-endopeptidase PBP7; and the cytoplasmic recycling enzymes ElsL and AmpD (red). Autolysin activity is shown at the 1,6-anhMurNAc end of the glycan chain, but it is not known from which ends MltF/Slt release the muropeptide. It is also possible that ElsL could act before NagZ. IM, inner membrane; Tpases, transpeptidase; GTase, glycosyltransferase.

encode PhoPQ, but analogous mechanisms are likely to contribute to cell envelope homeostasis to counter the turgor when the cell wall is compromised. One mechanism might include fortification of the cell envelope with lipoproteins, which occurs in *A. baumannii* during stress (42–44, 69); however, the underlying protective mechanism is not understood. Furthermore, noncovalent attachments between the outer membrane and PG network via OmpA and the hyperacylation of lipid A via LpxM may also increase the mechanical load-bearing capacity of the outer membrane to maintain envelope homeostasis when the cell wall is defective. It is also possible that disruption of OmpA or LpxM induced pleiotropic effects that reduced the barrier function to gate meropenem entry.

Unexpectedly, our data suggest that PG maintenance enzymes contribute to *A. baumannii* survival during meropenem treatment. Tetrapeptides represent the most abundant PG stem peptides in *A. baumannii*. They are formed, in part, by the DD-carboxypeptidase and DD-endopeptidase activity of PBP7 on pentapeptides and DD-cross-linked muropeptides, respectively (Fig. 4A). Tetrapeptides are substrates for LD-transpeptidase that form a small amount of 3-3 cross-links in *A. baumannii* (20) but are needed to effectively repair PG defects in stressed *E. coli* cells (2). Furthermore, tetrapeptides are also necessary for the LD-transpeptidase-dependent covalent attachment of Braun's lipoprotein (Lpp) to *m*DAP residues in PG (70), which also fortifies the *E. coli* envelope (1). Our data indicate that without PBP7, LdtJ-dependent 3-3 cross-link formation is reduced (Fig. 4A), suggesting that PBP7's role in cell envelope stability is related to its involvement in the 3-3 cross-link formation pathway. However, <3% of all muropeptides contain 3-3 cross-links, and their contributions to PG integrity maintenance remain unclear.

MltF and Slt were induced during meropenem treatment (Fig. 2 and 6), consistent with the activation of autolysins in response to penicillin-binding protein inhibition during β-lactam treatment (7, 17). Lytic transglycosylases cleave the glycosidic linkage

between disaccharide subunits within the PG strands and perform intramolecular transglycosylation in Mur*N*Ac to release soluble 1,6-anhydroMur*N*Ac-containing muropeptides, which can be imported into the cytoplasm. The main turnover product, 1,6-anhydro-MurNAc-tetrapeptide (TetraAnh), is transported into the cytoplasm by AmpG, where they provide the substrates for ElsL-dependent LD-carboxypeptidase activity to form TriAnh. Like other members of the YkuD family, ElsL retains a preference for tetrapeptide substrates (Fig. 5B) but represents the first known YkuD-containing enzyme that lacks a signal sequence and is active in the cytoplasm. ElsL is the second member of the YkuD family, after DpaA/LdtF, that has a major role in cleaving amide bonds rather than generating them. Notably, the requirement for ElsL in meropenem tolerance implies that cells depend on PG maintenance during spheroplast formation. Finally, ElsL (and LdtJ) was shown to be essential for *A. baumannii* survival without LOS (20), suggesting that PG recycling and modification of tetrapeptides are a general response to counter cell envelope stress in *A. baumannii*. It is also possible that the cytosolic accumulation of tetrapeptides somehow exacerbates mutant sickness.

The hydrolysis of TriAnh by the dedicated enzymes NagZ and AmpD results in the formation of anhMur*N*Ac-tripeptide and of 1,6-anhMur*N*Ac and tripeptides, respectively, and these fragments could be further degraded into individual amino acids for utilization as nutrient or energy sources (71–73) to promote survival during tolerance. It is reasonable to expect that the cell requires some nutrients during tolerance, and this pathway could provide energy to support basal metabolic processes. Alternatively, Mpl could ligate tripeptides to UDP-Mur*N*Ac in the recycling pathway (66, 74). UPD-Mur*N*Ac-tripeptide is an intermediate in the *de novo* PG synthesis pathway (75–77), and it is possible that the enhanced availability of PG precursors primes cells for efficient recovery when the antibiotic has been removed. Another possibility is that the accumulation of cytoplasmic 1,6-anhydroMur*N*Ac-containing muropeptides provides signals to induce $\beta$-lactamase expression, which could degrade meropenem. Notably, two mechanisms have been characterized in Gram-negative bacteria, including the AmpG-AmpR pathway and the BlrAB two-component system, both of which induce $\beta$-lactamase expression in response to muropeptide concentrations (78). While *A. baumannii* strain ATCC 17978 encodes both *Acinetobacter*-derived cephalosporinase (encoded by *A1S_2367*) and a putative OXA-51-like $\beta$-lactamase (encoded by *A1S_1517*), neither gene was upregulated in the transcriptomics analysis. It is also possible that one or both $\beta$-lactamases have low-level carbapenemase activity, which, when coupled with the observed downregulation of porins, might contribute sufficiently to meropenem degradation to promote survival. While many genes in *A. baumannii* have not yet been characterized, it is also possible that signaling pathways and potentially other carbapenemases could be induced in response to 1,6-anhydroMur*N*Ac-containing muropeptide accumulation to promote meropenem degradation. A more detailed analysis is needed to characterize the PG recycling tolerance mechanism, which will inform more effective treatment strategies to combat *A. baumannii* infections.

## MATERIALS AND METHODS

**Bacterial strains and growth.** All strains and plasmids used in this study are listed in Table S2 in the supplemental material. Primers are listed in Table S3. All *A. baumannii* strains were grown aerobically from freezer stocks on Luria-Bertani (LB) agar at 37°C. Antibiotics were used at the following concentrations unless noted otherwise: 25 mg/L kanamycin, 10 mg/L meropenem, 10 mg/L tetracycline, and 75 mg/L carbenicillin.

**Construction of genetic mutants.** *A. baumannii pbpG*, *ampD*, *ompA*, and *adeIJK* mutants were constructed as described previously (20, 54), using the recombination-mediated genetic engineering (recombineering) method (54). Briefly, a kanamycin resistance cassette flanked by FLP recombination target (FRT) sites was PCR amplified from the pKD4 plasmid using primers containing 125-bp flanking regions of homology to the gene of interest. The resulting linear PCR product was then transformed via electroporation into *A. baumannii* strain ATCC 17978 expressing pREC$_{Ab}$ (pAT03). Transformants were recovered in Luria broth and plated onto LB agar supplemented with 7.5 mg/L kanamycin. All genetic mutants were confirmed by PCR.

Following the isolation of genetic mutants, the pMMB67EH::REC$_{Ab}$ Tet$^r$ plasmid was removed as described previously (54). Isolated mutants were grown on LB agar supplemented with 2 mM nickel(II) chloride (NiCl$_2$) and replica plated onto LB agar supplemented with kanamycin or tetracycline. The loss

of the pMMB67EH::REC$_{Ab}$ Tet$^r$ plasmid in mutants susceptible to tetracycline and resistant to kanamycin was confirmed using PCR. To excise the chromosomal insertion of the kanamycin resistance cassette, cured mutants were transformed with pMMB67EH carrying the FLP recombinase (pAT08) and plated onto LB agar supplemented with tetracycline and 2 mM isopropyl $\beta$-D-1-thiogalactopyranoside (IPTG) to induce the expression of FLP recombinase. The successful excision of the kanamycin resistance cassette was confirmed using PCR.

The PBP7 complementation vector was constructed by amplifying the *pbpG* (*A1S_0237*) coding sequence (encoding PBP7) with 200-bp upstream and downstream flanking regions from *A. baumannii* ATCC 17978 genomic DNA (gDNA) and cloning it into the XhoI and KpnI restriction sites in the pABBRkn$^R$ plasmid. The resulting pPBP7 plasmid was transformed into the *A. baumannii* ATCC 17978 Δ*pbpG* background for complementation using the native promoter.

AmpD and OmpA complementation vectors were constructed similarly, with slight alterations. The *ampD* (*A1S_0045*) and *ompA* (*A1S_2840*) coding sequences were amplified from *A. baumannii* ATCC 17978 gDNA and cloned into the BamHI and SalI restriction sites in the pMMB67EHkn$^R$ plasmid. The resulting pAmpD and pOmpA plasmids were transformed into the respective mutants and induced with 2 mM IPTG for complementation.

**Fluorescent NADA staining.** Cultures were grown overnight with shaking at 37°C in 5 mL of BHI (Bacto brain heart infusion) broth (BD Difco). The following day, cultures were back-diluted at 1:10 in fresh BHI medium (total volume of 5 mL) without or with meropenem. Two microliters of 10 mM NBD-(linezolid-7-nitrobenz-2-oxa-1,3-diazol-4-yl)-amino-D-alanine (NADA) (Thermo Fisher) was added to each tube, and the mixture was incubated at 37°C. At 0, 6, and 12 h, cultures (5 mL) were washed twice in BHI broth and fixed with phosphate-buffered saline (PBS) containing a 1:10 solution of 16% paraformaldehyde. For spheroplast recovery, 12-h-treated cultures were washed 3 times in BHI broth to remove the excess meropenem and resuspended in fresh BHI broth. A total of 10 mM NADA was added, and the mixture was incubated for 12 h at 37°C before fixing the cells for microscopy.

**Microscopy.** Paraformaldehyde-fixed cells were immobilized on 1.5% agarose pads and imaged using an inverted Nikon Eclipse Ti-2 wide-field epifluorescence microscope equipped with a Photometrics Prime 95B camera and a Plan Apo 100× 1.45-numerical-aperture lens objective. Phase-contrast and fluorescence images were collected with NIS Elements software. Green fluorescence images were taken using a Sola light-emitting diode (LED) light engine and a filter cube with 632/60- or 535/50-nm emission filters.

**Image analysis.** Microscopy images were processed and pseudocolored with ImageJ Fiji (79). A cyan lookup table was applied to NADA images. Cell shape (length, width, and fluorescence intensities) and total cell surface area were quantified in MicrobeJ (80), and data were plotted in Prism 9 (GraphPad 9.2.0). Each experiment was independently replicated three times, data from one representative experiment are reported for quantification, and one representative image is included in the figures.

**RNA sequencing.** Transcriptome sequencing analysis was performed as described previously, with modification (42). Briefly, the Direct-Zol RNA miniprep kit (Zymo Research) was used to extract total RNA from *A. baumannii* ATCC 17978 cultures treated with either meropenem or an equivalent volume of water as a blank at 0.5, 3, and 9 h at 37°C in triplicate. A Turbo DNA-free DNA removal kit (Invitrogen) was used to remove genomic DNA contamination. DNase-depleted RNA was sent to the Microbial Genome Sequencing Center (MiGS) for Illumina NextSeq 550 sequencing. CLC genomic workbench software (Qiagen) was used to align the resulting sequencing data to the *A. baumannii* ATCC 17978 genome annotations and determine the reads per kilobase per million (RPKM) expression values and the weighted-proportions fold changes in expression values between meropenem-treated and untreated samples. Baggerley's test on proportions was used to generate a false discovery rate-adjusted $P$ value. The weighted-proportions fold change in expression values between samples was used to generate pathway-specific heat maps in Prism 9.

**Transposon insertion sequencing.** Transposon sequencing was performed as described previously (20, 42, 48, 81). Briefly, pJNW684 was conjugated into wild-type *A. baumannii* strain ATCC 17978 to generate a library of ~400,000 mutants. The transposon mutant library was pooled and screened for survival with and without meropenem treatment at 6, 9, and 12 h at 37°C. gDNA from meropenem-treated and untreated cultures was isolated and sheared, and transposon junctions were amplified and sequenced. The frequencies of transposon insertions were compared between meropenem-treated and untreated conditions to determine fitness determinants that contribute to carbapenem tolerance in *A. baumannii*.

**Time-dependent killing assays.** Meropenem killing experiments were performed as previously described, with slight alterations (21). Wild-type, mutant, and complementation strains were grown overnight in Luria broth at 37°C. The following day, cultures grown overnight were back-diluted at 1:10 in fresh, prewarmed BHI broth containing meropenem or an equivalent volume of water. Diluted BHI broth cultures were then incubated at 37°C. At 0, 3, 6, 12, and 24 h, each sample was diluted 4-fold in blank BHI broth, and the optical density at 600 nm (OD$_{600}$) was measured. At each time point, cells were serially diluted 10-fold in fresh BHI broth, and either 5 $\mu$L of each serial dilution was spot plated or 100 $\mu$L of each dilution was plated onto LB agar. Spot plates were imaged and CFU were calculated after 24 h at 37°C. Each experiment was independently replicated three times, and one representative data set is reported.

**Construction of PBP7 and ElsL active-site mutants.** Site-directed mutagenesis was performed, as previously described, with *elsL* (*A1S_2806*) (20). Briefly, the *pbpG* coding sequence was amplified from *A. baumannii* ATCC 17978 gDNA, cloned into the BamHI restriction site in pUC19, and transformed into *E. coli* C2987 chemically competent cells (New England BioLabs, Inc.). pUC19::*pbpG* was used as a template for *Pfu*-mediated deletion mutagenesis. DpnI-digested PCR mixtures were transformed into *E. coli* C2987

chemically competent cells and plated onto LB agar supplemented with 75 mg/L carbenicillin. All mutants were confirmed by PCR and Sanger sequencing.

**Construction of PBP7 and ElsL overexpression strains.** *pbpG* and *elsL* coding sequences were amplified from *A. baumannii* ATCC 17978 gDNA, and *pbpG*$_{S131A}$ and *elsL*$_{C138S}$ were amplified from pUC19:: *pbpG*$_{S131A}$ and pUC19::*elsL*$_{C138S}$ plasmid DNA using primers containing a His8× tag sequence. Amplicons were cloned into the NdeI and BamHI restriction sites in pT7-7Kn and transformed into *E. coli* C2987 chemically competent cells, resulting in pT7-7Kn::*pbpG*, pT7-7Kn::*pbpG*$_{S131A}$, pT7-7Kn::*elsL*, and pT7-7Kn:: *elsL*$_{C138S}$. Constructs were confirmed using Sanger sequencing and transformed into chemically competent *E. coli* C2527(BL21) cells (New England BioLabs, Inc.) for purification, expression, and Western blotting.

**Purification of recombinant PBP7 and ElsL.** BL21 cells carrying pT7-7Kn::*pbpG*, pT7-7Kn::*pbpG*$_{S131A}$, pT7-7Kn::*elsL*, and pT7-7Kn::*elsL*$_{C138S}$ were grown in 500 mL Luria broth with 1 mM IPTG at 37°C for 7 h. Cells were collected, washed in cold 1× PBS, and pelleted, and the supernatant was removed. The dry pellet was frozen at −80°C overnight. The pellet was thawed on ice and resuspended in 20 mL lysis buffer (20 mM Tris, 300 mM NaCl, 10 mM imidazole [pH 8]). Samples were sonicated for 20 s on and off for 10 min at 60% amplitude (Qsonica Q125 sonicator). Cells were centrifuged at 20,000 × *g* for 0.5 h at 4°C. The supernatant was incubated with lysis buffer-washed HisPur Ni-nitrilotriacetic acid (NTA) resin (Thermo Scientific) on a rotator for 2 h at 4°C. The sample was added to a 10-mL protein purification column containing a porous polyethylene disk (Thermo Scientific) and allowed to gravity drip. The column was washed three times with 20 mL lysis buffer and increasing concentrations of additional imidazole at each wash (0 mM, 15 mM, and 30 mM). Five hundred microliters of elution buffer (20 mM Tris, 300 mM NaCl, 250 mM imidazole [pH 8]) was incubated with the column for 5 min and then gravity eluted 9 times. The elution fractions containing protein, as determined by a protein gel, were injected into a 10-mW dialysis cassette (Thermo Scientific) and dialyzed overnight in dialysis buffer (10 mM Tris, 50 mM KCl, 0.1 mM EDTA, 5% glycerol [pH 8]) at 4°C. Purified protein was collected and verified by Western blotting with an anti-His antibody.

**Isolation of outer membrane vesicles.** Outer membrane vesicles were isolated as described previously (20). Briefly, cultures grown overnight were back-diluted to an OD$_{600}$ of 0.01 in 100 mL Luria broth and grown to stationary phase at 37°C. Cultures were then pelleted at 5,000 × *g* for 15 min at room temperature, and the supernatant was filtered through a 0.45-mm bottle-top filter. The filtered supernatant was ultracentrifuged (Sorvall WX 80+ ultracentrifuge with an AH-629 swinging-bucket rotor) at 151,243 × *g* for 1 h at 4°C. Following a final ultracentrifugation step, the outer membrane vesicle pellet was resuspended in 500 mL cold membrane vesicle buffer (50 mM Tris, 5 mM NaCl, 1 mM MgSO$_4$ [pH 7.5]). The isolation of outer membrane vesicles was repeated three times in duplicate; one representative data set is reported.

**Quantification of total outer membrane vesicle proteins.** A Bradford assay was used to determine outer membrane vesicle protein concentrations, as previously described (20). To generate a standard curve, bovine serum albumin (BSA) was diluted at 0 to 20 mg/mL in Pierce Coomassie Plus assay reagent (Thermo Fisher) to a final volume of 1 mL. Outer membrane vesicles were diluted at 2, 5, 10, 15, and 20 $\mu$L in reagent to a final volume of 1 mL. A microplate spectrophotometer (Fisherbrand AccuSkan) was used to measure the absorbance (OD$_{595}$) of the standard and samples in a 96-well plate (BrandTech). Protein concentrations were determined by comparing the optical densities of the samples to the standard curve plotted in Microsoft Excel, and final quantifications were graphed in GraphPad Prism 9. Experiments were reproduced three times from each outer membrane vesicle isolation, and one representative data set is reported.

**Quantification of outer membrane vesicle Kdo concentrations.** 3-Deoxy-D-manno-oct-2-ulosonic acid (Kdo) assays were carried out as described previously (20, 82). For the standard curve, the Kdo standard (Sigma) was diluted at 0 to 128 $\mu$g/mL in 50 $\mu$L of deionized (DI) water. Fifty microliters of 0.5 M sulfuric acid (H$_2$SO$_4$) was added to 50 $\mu$L of isolated outer membrane vesicles and freshly prepared 50-$\mu$L dilutions of the Kdo standard. Outer membrane versicles in 0.5 M H$_2$SO$_4$ were boiled for 8 min to release the Kdo sugars. Samples were allowed to cool for 10 min at room temperature. Fifty microliters of 0.1 M periodic acid was added to outer membrane vesicles and Kdo standards, and the mixture was incubated at room temperature for 10 min. Following incubation, 200 $\mu$L of 0.2 M sodium arsenite in 0.5 M hydrochloric acid (HCl) was added to outer membrane vesicles and Kdo standards, followed by 800 $\mu$L of 0.6% freshly prepared thiobarbituric acid (TBA). All samples were boiled for 10 min and allowed to cool at room temperate for 30 to 40 min. Prior to optical density measurements, purified Kdo was extracted using *n*-butanol equilibrated with 0.5 M HCl. The optical density was measured at 552 nm and 509 nm (Fisherbrand AccuSkan microplate spectrophotometer) in disposable polystyrene cuvettes (Fisherbrand). A linear Kdo standard curve was generated by subtracting OD$_{552}$ measurements from OD$_{509}$ measurements in Microsoft Excel, and final quantifications were graphed in GraphPad Prism 9. Experiments were reproduced three times from each outer membrane vesicle isolation, and one representative data set is reported.

**Ethidium bromide permeability assay.** Permeability assays were done as previously described (83), with slight modifications. Briefly, cultures were grown overnight in 5 mL BHI medium, normalized, and back-diluted (1:10) in BHI medium with and without meropenem. Cultures were withdrawn at 0, 6, and 12 h; washed 3 times with PBS; and normalized based on the OD$_{600}$. One hundred eighty milliliters of the cultures was added to a 96-well black plate, and 6 $\mu$M EtBr was added immediately before fluorescence measurements. The relative fluorescence units (RFU) were analyzed using a synergy multimode plate reader (530-nm excitation filter, 590-nm emission filter, and 570-nm dichroic mirror). The temperature was adjusted to 25°C, and the results were read at 15-s intervals for 0.5 h. Assays were repeated

three times in triplicate; one representative data set is reported. The mean RFU for each sample were calculated and plotted using Prism 9. Experiments were reproduced three times, and one representative data set is reported.

**PG isolation.** Biological replicates were grown to mid-logarithmic or stationary phase in 400 mL of Luria broth. Cells were centrifuged (Avanti JXN-26 Beckman Coulter centrifuge and Beckman Coulter JA-10 rotor) at 7,000 × *g* for 0.5 h at 4°C, resuspended in chilled 6 mL PBS, and lysed via dropwise addition to boiling 8% sodium dodecyl sulfate (SDS). PG was further purified as previously described (84). Briefly, muropeptides were cleaved from PG by Cellosyl muramidase (Hoechst, Frankfurt am Main, Germany), reduced with sodium borohydride, and separated on a 250- by 4.6-mm 3-$\mu$m Prontosil 120-3-$C_{18}$ AQ reversed-phase column (Bischoff, Leonberg, Germany). The eluted muropeptides were detected by the absorbance at 205 nm. Eluted peaks were designated based on known published chromatograms (20, 42, 57); new peaks were analyzed by MS/MS, as previously described (20).

**Activity assays.** PBP7 activity assays were carried out in a final volume of 50 $\mu$L containing 20 mM HEPES (pH 5.0, 6.0, or 7.5), 50 mM NaCl, and 2 $\mu$M PBP7 or PBP7$_{S131A}$. PG from *E. coli* D456 was added, and the reaction mixture was incubated at 37°C for 16 h. The reaction was stopped by boiling the samples for 10 min. The reaction mixture was reduced with sodium borohydride and acidified to pH 4.0 to 4.5. *E. coli* D456 PG under pH 5.0 buffer conditions served as a control. Muropeptides were analyzed as previously described (84).

ElsL activity assays were carried out in a final volume of 50 $\mu$L containing 20 mM NaP (pH 5.0) and 10 $\mu$M ElsL or ElsL$_{C138S}$. PG from *E. coli* BW25113 (WT) (tetra-muropeptide rich) or CS703-1 (multiple mutations in penicillin-binding proteins) (penta-muropeptide rich) was added, and the reaction mixture was incubated at 37°C for 4 h. The reaction was stopped by boiling the samples for 10 min. Muropeptides were reduced with sodium borohydride. Muropeptides were analyzed as previously described (84).

**Cell fractionation.** Cells were grown to mid-logarithmic or stationary phase and normalized to an $OD_{600}$ of 0.75 in 20 mL. Cultures were washed twice with chilled 1× PBS plus 0.1% gelatin (PBSG), resuspended in 2 mL chilled PBSG containing 2 mg/mL polymyxin B sulfate (MilliporeSigma), and then agitated for 0.5 h at 4°C. Spheroplasts were pelleted at 20,000 × *g* for 0.5 h at 4°C. The remaining supernatant was centrifuged at 20,000 × *g* for 0.5 h at 4°C. The supernatant was collected and saved as the periplasmic fraction. Previously pelleted spheroplasts were resuspended in 1 mL 10 mM HEPES buffer solution (Gibco), and 100 $\mu$L was collected as whole spheroplasts. The remaining spheroplasts were sonicated for 15 s on and 15 s off 10 times at 60% amplitude (Qsonica Q125 sonicator). Lysed spheroplasts were pelleted at 16,000 × *g* for 0.5 h at 4°C. The supernatant was centrifuged for another 0.5 h at 16,000 × *g* at 4°C. The insoluble pellet was saved as the total membrane fraction. The soluble supernatant was saved as the cytoplasmic fraction. Experiments were reproduced three times, and one representative data set is reported.

**Immunoblot assays.** ElsL, OmpA, and RpoA polyclonal antibodies were generated (Thermo Fisher Scientific) from rabbit immunization with peptide fragments. Briefly, a 20-amino-acid peptide from ElsL (ELFDLVSEDALVYLSEQSLT), a 19-amino-acid peptide from OmpA (KEGRAMNRRVFATITGSR), and a 19-amino-acid peptide from RpoA (ENWPPASLRMDDRFAYRSR) predicted to be solvent exposed were selected from the primary sequence of *A. baumannii* ATCC 17978, synthesized, and used to generate each specific antibody from rabbits. The collected serum was tested for reactivity in an enzyme-linked immunosorbent assay (ELISA) with peptide fragments and via Western blotting against whole-cell lysates.

All Western blot analyses were performed using 4 to 12% Bis-Tris 10-well protein gels (Invitrogen) and NuPage morpholineethanesulfonic acid (MES) SDS running buffer (Novex). Gels were transferred with NuPage transfer buffer (Novex) to 0.45-$\mu$m polyvinylidene difluoride (PVDF) membranes (Amersham Hybond). All blots were blocked in 5% milk and 1× Tris-buffered saline (TBS) for 2 h. For primary rabbit antisera, anti-ElsL and anti-RpoA were used at a 1:750 dilution, while anti-OmpA was used at 1:1,000. Anti-rabbit horseradish peroxidase (HRP) secondary antibody was used at 1:10,000 (Thermo Fisher Scientific). The penta-his primary anti-mouse antibody was used at 1:500 (Invitrogen). Anti-mouse HRP secondary antibody was used at 1:10,000 (Invitrogen). SuperSignal West Pico Plus (Thermo Fisher Scientific) was applied to detect relative protein concentrations.

For localization assays, whole-cell lysates, whole spheroplasts, and membrane fractions were mixed with 1× loading dye containing 4% 2-mercaptoethanol (Fisher Chemical) and boiled for 10 min. Ten microliters of each sample was used. One hundred thirty-two microliters of the periplasmic or cytoplasmic fraction was added to 66 $\mu$L of 3× loading buffer containing 4% 2-mercaptoethanol (Fisher Chemical) and boiled for 10 min. Sixty microliters of each sample was used. Each sample was loaded into 4 to 12% Bis-Tris 10-well protein gels (Invitrogen) for immunoblotting.

For protein purification, 1 $\mu$g of purified protein was combined with 3× loading buffer containing 4% 2-mercaptoethanol and boiled for 10 min. The sample was loaded into a 4 to 12% Bis-Tris 10-well protein gel (Invitrogen) for immunoblotting.

**MIC determination.** MICs were determined using the broth microdilution (BMD) method, as previously outlined (85). Cultures grown overnight were back-diluted to an $OD_{600}$ of 0.01, and 100 $\mu$L of cells was added to each well of a 96-well round-bottom polypropylene plate (Grenier Bio-One). Meropenem diluted in water was serially diluted, and 150 $\mu$L of each meropenem serial dilution was also added to each well. Plates were incubated overnight at 37°C, and growth was measured by reading the $OD_{600}$ after 24 h of incubation. The lowest concentration of meropenem at which no bacterial growth was observed was determined to be the MIC. Assays were repeated three times in triplicate; one representative data set is reported.

**Statistical analysis.** Tests for significance in cell morphology, fluorescence intensity, and outer membrane vesicle production were conducted using Student's *t* test (two-tailed distribution with two-sample, equal-variance calculations). Statistically significant differences between relevant strains possessed *P* values of <0.05.

**Data availability.** The sequencing data have been deposited in the National Center for Biotechnology Information's Gene Expression Omnibus (accession number GSE190441).

## SUPPLEMENTAL MATERIAL

Supplemental material is available online only.

**FIG S1**, TIF file, 0.9 MB.
**FIG S2**, TIF file, 1.7 MB.
**FIG S3**, TIF file, 2.1 MB.
**FIG S4**, TIF file, 0.5 MB.
**FIG S5**, TIF file, 0.4 MB.
**TABLE S1**, DOCX file, 0.02 MB.
**TABLE S2**, DOCX file, 0.03 MB.
**TABLE S3**, DOCX file, 0.02 MB.

## ACKNOWLEDGMENTS

## REFERENCES

1. Rojas ER, Billings G, Odermatt PD, Auer GK, Zhu L, Miguel A, Chang F, Weibel DB, Theriot JA, Huang KC. 2018. The outer membrane is an essential load-bearing element in Gram-negative bacteria. Nature 559:617–621. https://doi.org/10.1038/s41586-018-0344-3.
2. Morè N, Martorana AM, Biboy J, Otten C, Winkle M, Serrano CKG, Montón Silva A, Atkinson L, Yau H, Breukink E, den Blaauwen T, Vollmer W, Polissi A. 2019. Peptidoglycan remodeling enables Escherichia coli to survive severe outer membrane assembly defect. mBio 10:e02729-18. https://doi.org/10.1128/mBio.02729-18.
3. Levin-Reisman I, Ronin I, Gefen O, Braniss I, Shoresh N, Balaban NQ. 2017. Antibiotic tolerance facilitates the evolution of resistance. Science 355:826–830. https://doi.org/10.1126/science.aaj2191.
4. Levin-Reisman I, Brauner A, Ronin I, Balaban NQ. 2019. Epistasis between antibiotic tolerance, persistence, and resistance mutations. Proc Natl Acad Sci U S A 116:14734–14739. https://doi.org/10.1073/pnas.1906169116.
5. Liu J, Gefen O, Ronin I, Bar-Meir M, Balaban NQ. 2020. Effect of tolerance on the evolution of antibiotic resistance under drug combinations. Science 367:200–204. https://doi.org/10.1126/science.aay3041.
6. Brauner A, Fridman O, Gefen O, Balaban NQ. 2016. Distinguishing between resistance, tolerance and persistence to antibiotic treatment. Nat Rev Microbiol 14:320–330. https://doi.org/10.1038/nrmicro.2016.34.
7. Dörr T. 2021. Understanding tolerance to cell wall-active antibiotics. Ann N Y Acad Sci 1496:35–58. https://doi.org/10.1111/nyas.14541.
8. Westblade LF, Errington J, Dörr T. 2020. Antibiotic tolerance. PLoS Pathog 16:e1008892. https://doi.org/10.1371/journal.ppat.1008892.
9. Papp-Wallace KM, Endimiani A, Taracila MA, Bonomo RA. 2011. Carbapenems: past, present, and future. Antimicrob Agents Chemother 55:4943–4960. https://doi.org/10.1128/AAC.00296-11.
10. Bassetti M, Nicolini L, Esposito S, Righi E, Viscoli C. 2009. Current status of newer carbapenems. Curr Med Chem 16:564–575. https://doi.org/10.2174/092986709787458498.
11. Torres JA, Villegas MV, Quinn JP. 2007. Current concepts in antibiotic-resistant gram-negative bacteria. Expert Rev Anti Infect Ther 5:833–843. https://doi.org/10.1586/14787210.5.5.833.
12. Paterson DL, Bonomo RA. 2005. Extended-spectrum beta-lactamases: a clinical update. Clin Microbiol Rev 18:657–686. https://doi.org/10.1128/CMR.18.4.657-686.2005.
13. Eliopoulos GM, Maragakis LL, Perl TM. 2008. Acinetobacter baumannii: epidemiology, antimicrobial resistance, and treatment options. Clin Infect Dis 46:1254–1263. https://doi.org/10.1086/529198.
14. Rahal JJ. 2009. Antimicrobial resistance among and therapeutic options against gram-negative pathogens. Clin Infect Dis 49(Suppl 1):S4–S10. https://doi.org/10.1086/599810.
15. CDC. 2019. Antibiotic resistance threats in the United States, 2019. CDC, Atlanta, GA.
16. WHO. 2017. Global priority list of antibiotic-resistant bacteria to guide research, discovery, and development of new antibiotics. WHO, Geneva, Switzerland. https://www.quotidianosanita.it/allegati/allegato4135670.pdf. Accessed 1 January 2018.
17. Dörr T, Davis BM, Waldor MK. 2015. Endopeptidase-mediated beta lactam tolerance. PLoS Pathog 11:e1004850. https://doi.org/10.1371/journal.ppat.1004850.
18. Weaver AI, Murphy SG, Umans BD, Tallavajhala S, Onyekwere I, Wittels S, Shin J-H, VanNieuwenhze M, Waldor MK, Dörr T. 2018. Genetic determinants of penicillin tolerance in Vibrio cholerae. Antimicrob Agents Chemother 62:e01326-18. https://doi.org/10.1128/AAC.01326-18.
19. Monahan LG, Turnbull L, Osvath SR, Birch D, Charles IG, Whitchurch CB. 2014. Rapid conversion of Pseudomonas aeruginosa to a spherical cell morphotype facilitates tolerance to carbapenems and penicillins but increases susceptibility to antimicrobial peptides. Antimicrob Agents Chemother 58:1956–1962. https://doi.org/10.1128/AAC.01901-13.
20. Kang KN, Kazi MI, Biboy J, Gray J, Bovermann H, Ausman J, Boutte CC, Vollmer W, Boll JM. 2021. Septal class A penicillin-binding protein activity and LD-transpeptidases mediate selection of colistin-resistant lipooligosaccharide-deficient Acinetobacter baumannii. mBio 12:e02185-20. https://doi.org/10.1128/mBio.02185-20.
21. Cross T, Ransegnola B, Shin J-H, Weaver A, Fauntleroy K, VanNieuwenhze MS, Westblade LF, Dörr T. 2019. Spheroplast-mediated carbapenem tolerance in Gram-negative pathogens. Antimicrob Agents Chemother 63:e00756-19. https://doi.org/10.1128/AAC.00756-19.
22. Murtha AN, Kazi MI, Schargel RD, Cross T, Fihn C, Cattoir V, Carlson EE, Boll JM, Dörr T. 2022. High-level carbapenem tolerance requires antibiotic-induced outer membrane modifications. PLoS Pathog 18:e1010307. https://doi.org/10.1371/journal.ppat.1010307.
23. McLeod GI, Spector MP. 1996. Starvation- and stationary-phase-induced resistance to the antimicrobial peptide polymyxin B in Salmonella typhimurium is RpoS ($\sigma^S$) independent and occurs through both phoP-dependent and -independent pathways. J Bacteriol 178:3683–3688. https://doi.org/10.1128/jb.178.13.3683-3688.1996.
24. Tuomanen E, Cozens R, Tosch W, Zak O, Tomasz A. 1986. The rate of killing of Escherichia coli by beta-lactam antibiotics is strictly proportional to

the rate of bacterial growth. J Gen Microbiol 132:1297–1304. https://doi
.org/10.1099/00221287-132-5-1297.

25. Lee AJ, Wang S, Meredith HR, Zhuang B, Dai Z, You L. 2018. Robust, linear correlations between growth rates and $\beta$-lactam-mediated lysis rates. Proc Natl Acad Sci U S A 115:4069–4074. https://doi.org/10.1073/pnas .1719504115.

26. Kuru E, Lambert C, Rittichier J, Till R, Ducret A, Derouaux A, Gray J, Biboy J, Vollmer W, VanNieuwenhze M, Brun YV, Sockett RE. 2017. Fluorescent D-amino-acids reveal bi-cellular cell wall modifications important for Bdello-vibrio bacteriovorus predation. Nat Microbiol 2:1648–1657. https://doi .org/10.1038/s41564-017-0029-y.

27. Kuru E, Radkov A, Meng X, Egan A, Alvarez L, Dowson A, Booher G, Breukink E, Roper DI, Cava F, Vollmer W, Brun Y, VanNieuwenhze MS. 2019. Mechanisms of incorporation for D-amino acid probes that target peptidoglycan biosynthesis. ACS Chem Biol 14:2745–2756. https://doi .org/10.1021/acschembio.9b00664.

28. Baranowski C, Welsh MA, Sham L-T, Eskandarian HA, Lim HC, Kieser KJ, Wagner JC, McKinney JD, Fantner GE, Ioerger TR, Walker S, Bernhardt TG, Rubin EJ, Rego EH. 2018. Maturing Mycobacterium smegmatis peptido-glycan requires non-canonical crosslinks to maintain shape. Elife 7: e37516. https://doi.org/10.7554/eLife.37516.

29. García-Heredia A, Pohane AA, Melzer ES, Carr CR, Fiolek TJ, Rundell SR, Lim HC, Wagner JC, Morita YS, Swarts BM, Siegrist MS. 2018. Peptidogly-can precursor synthesis along the sidewall of pole-growing mycobacteria. Elife 7:e37243. https://doi.org/10.7554/eLife.37243.

30. Lin M-F, Lin Y-Y, Tu C-C, Lan C-Y. 2017. Distribution of different efflux pump genes in clinical isolates of multidrug-resistant Acinetobacter bau-mannii and their correlation with antimicrobial resistance. J Microbiol Immunol Infect 50:224–231. https://doi.org/10.1016/j.jmii.2015.04.004.

31. Yoon E-J, Courvalin P, Grillot-Courvalin C. 2013. RND-type efflux pumps in multidrug-resistant clinical isolates of Acinetobacter baumannii: major role for AdeABC overexpression and AdeRS mutations. Antimicrob Agents Chemother 57:2989–2995. https://doi.org/10.1128/AAC.02556-12.

32. Rajamohan G, Srinivasan VB, Gebreyes WA. 2010. Novel role of Acineto-bacter baumannii RND efflux transporters in mediating decreased sus-ceptibility to biocides. J Antimicrob Chemother 65:228–232. https://doi .org/10.1093/jac/dkp427.

33. Damier-Piolle L, Magnet S, Brémont S, Lambert T, Courvalin P. 2008. AdeIJK, a resistance-nodulation-cell division pump effluxing multiple antibiotics in Acinetobacter baumannii. Antimicrob Agents Chemother 52:557–562. https://doi.org/10.1128/AAC.00732-07.

34. Kornelsen V, Kumar A. 2021. Update on multidrug resistance efflux pumps in Acinetobacter spp. Antimicrob Agents Chemother 65:e00514-21. https://doi.org/10.1128/AAC.00514-21.

35. Pagès J-M, James CE, Winterhalter M. 2008. The porin and the permeating antibiotic: a selective diffusion barrier in Gram-negative bacteria. Nat Rev Microbiol 6:893–903. https://doi.org/10.1038/nrmicro1994.

36. Mussi MA, Relling VM, Limansky AS, Viale AM. 2007. CarO, an Acineto-bacter baumannii outer membrane protein involved in carbapenem re-sistance, is essential for L-ornithine uptake. FEBS Lett 581:5573–5578. https://doi.org/10.1016/j.febslet.2007.10.063.

37. Mussi MA, Limansky AS, Viale AM. 2005. Acquisition of resistance to carba-penems in multidrug-resistant clinical strains of Acinetobacter baumannii: natural insertional inactivation of a gene encoding a member of a novel family of beta-barrel outer membrane proteins. Antimicrob Agents Chemo-ther 49:1432–1440. https://doi.org/10.1128/AAC.49.4.1432-1440.2005.

38. Dupont M, Pagès J-M, Lafitte D, Siroy A, Bollet C. 2005. Identification of an OprD homologue in Acinetobacter baumannii. J Proteome Res 4:2386–2390. https://doi.org/10.1021/pr050143q.

39. Catel-Ferreira M, Marti S, Guillon L, Jara L, Coadou G, Molle V, Bouffartigues E, Bou G, Shalk I, Jouenne T, Vila-Farrés X, Dé E. 2016. The outer membrane porin OmpW of Acinetobacter baumannii is involved in iron uptake and col-istin binding. FEBS Lett 590:224–231. https://doi.org/10.1002/1873-3468 .12050.

40. Shin J-H, Choe D, Ransegnola B, Hong H-R, Onyekwere I, Cross T, Shi Q, Cho B-K, Westblade LF, Brito IL, Dörr T. 2021. A multifaceted cellular dam-age repair and prevention pathway promotes high-level tolerance to $\beta$-lactam antibiotics. EMBO Rep 22:e51790. https://doi.org/10.15252/ embr.202051790.

41. Dörr T, Alvarez L, Delgado F, Davis BM, Cava F, Waldor MK. 2016. A cell wall damage response mediated by a sensor kinase/response regulator pair enables beta-lactam tolerance. Proc Natl Acad Sci U S A 113:404–409. https://doi.org/10.1073/pnas.1520333113.

42. Boll JM, Crofts AA, Peters K, Cattoir V, Vollmer W, Davies BW, Trent MS. 2016. A penicillin-binding protein inhibits selection of colistin-resistant, lipooligosaccharide-deficient Acinetobacter baumannii. Proc Natl Acad Sci U S A 113:E6228–E6237. https://doi.org/10.1073/pnas.1611594113.

43. Henry R, Vithanage N, Harrison P, Seemann T, Coutts S, Moffatt JH, Nation RL, Li J, Harper M, Adler B, Boyce JD. 2012. Colistin-resistant, lipopolysac-charide-deficient Acinetobacter baumannii responds to lipopolysacchar-ride loss through increased expression of genes involved in the synthesis and transport of lipoproteins, phospholipids, and poly-$\beta$-1,6-N-acetylglu-cosamine. Antimicrob Agents Chemother 56:59–69. https://doi.org/10 .1128/AAC.05191-11.

44. Henry R, Crane B, Powell D, Deveson Lucas D, Li Z, Aranda J, Harrison P, Nation RL, Adler B, Harper M, Boyce JD, Li J. 2015. The transcriptomic response of Acinetobacter baumannii to colistin and doripenem alone and in combination in an in vitro pharmacokinetics/pharmacodynamics model. J Antimicrob Chemother 70:1303–1313. https://doi.org/10.1093/ jac/dku536.

45. Mathelié-Guinlet M, Asmar AT, Collet J-F, Dufrêne YF. 2020. Lipoprotein Lpp regulates the mechanical properties of the E. coli cell envelope. Nat Commun 11:1789. https://doi.org/10.1038/s41467-020-15489-1.

46. Cho H, Uehara T, Bernhardt TG. 2014. Beta-lactam antibiotics induce a le-thal malfunctioning of the bacterial cell wall synthesis machinery. Cell 159:1300–1311. https://doi.org/10.1016/j.cell.2014.11.017.

47. Weaver AI, Alvarez L, Rosch KM, Ahmed A, Wang GS, van Nieuwenhze MS, Cava F, Dörr T. 2022. Lytic transglycosylases mitigate periplasmic crowd-ing by degrading soluble cell wall turnover products. Elife 11:e73178. https://doi.org/10.7554/eLife.73178.

48. Kazi MI, Schargel RD, Boll JM. 2020. Generating transposon insertion libra-ries in Gram-negative bacteria for high-throughput sequencing. J Vis Exp 2020:e61612. https://doi.org/10.3791/61612.

49. Park JS, Lee WC, Yeo KJ, Ryu K-S, Kumarasiri M, Hesek D, Lee M, Mobashery S, Song JH, Kim SI, Lee JC, Cheong C, Jeon YH, Kim H-Y. 2012. Mechanism of anchoring of OmpA protein to the cell wall peptidoglycan of the gram-negative bacterial outer membrane. FASEB J 26:219–228. https://doi.org/10.1096/fj.11-188425.

50. Gribun A, Nitzan Y, Pechatnikov I, Hershkovits G, Katcoff DJ. 2003. Molecu-lar and structural characterization of the HMP-AB gene encoding a pore-forming protein from a clinical isolate of Acinetobacter baumannii. Curr Microbiol 47:434–443. https://doi.org/10.1007/s00284-003-4050-4.

51. Smani Y, McConnell MJ, Pachón J. 2012. Role of fibronectin in the adhe-sion of Acinetobacter baumannii to host cells. PLoS One 7:e33073. https://doi.org/10.1371/journal.pone.0033073.

52. Tsai Y-K, Liou C-H, Lin J-C, Fung C-P, Chang F-Y, Siu LK. 2020. Effects of dif-ferent resistance mechanisms on antimicrobial resistance in Acineto-bacter baumannii: a strategic system for screening and activity testing of new antibiotics. Int J Antimicrob Agents 55:105918. https://doi.org/10 .1016/j.ijantimicag.2020.105918.

53. Moon DC, Choi CH, Lee JH, Choi C-W, Kim H-Y, Park JS, Kim SI, Lee JC. 2012. Acinetobacter baumannii outer membrane protein A modulates the biogenesis of outer membrane vesicles. J Microbiol 50:155–160. https://doi.org/10.1007/s12275-012-1589-4.

54. Boll JM, Tucker AT, Klein DR, Beltran AM, Brodbelt JS, Davies BW, Trent MS. 2015. Reinforcing lipid A acylation on the cell surface of Acinetobacter bau-mannii promotes cationic antimicrobial peptide resistance and desiccation survival. mBio 6:e00478-15. https://doi.org/10.1128/mBio.00478-15.

55. Horne JE, Brockwell DJ, Radford SE. 2020. Role of the lipid bilayer in outer membrane protein folding in Gram-negative bacteria. J Biol Chem 295: 10340–10367. https://doi.org/10.1074/jbc.REV120.011473.

56. Storek KM, Auerbach MR, Shi H, Garcia NK, Sun D, Nickerson NN, Vij R, Lin Z, Chiang N, Schneider K, Wecksler AT, Skippington E, Nakamura G, Seshasayee D, Koerber JT, Payandeh J, Smith PA, Rutherford ST. 2018. Monoclonal antibody targeting the $\beta$-barrel assembly machine of Esche-richia coli is bactericidal. Proc Natl Acad Sci U S A 115:3692–3697. https:// doi.org/10.1073/pnas.1800043115.

57. Le N-H, Peters K, Espaillat A, Sheldon JR, Gray J, Di Venanzio G, Lopez J, Djahanschiri B, Mueller EA, Hennon SW, Levin PA, Ebersberger I, Skaar EP, Cava F, Vollmer W, Feldman MF. 2020. Peptidoglycan editing provides im-munity to Acinetobacter baumannii during bacterial warfare. Sci Adv 6: eabb5614. https://doi.org/10.1126/sciadv.abb5614.

58. Edwards DH, Donachie WD. 1993. Construction of a triple deletion of pen-icillin-binding proteins 4, 5, and 6 in Escherichia coli, p 369–374. In de Pedro MA, Höltje J-V, Löffelhardt W (ed), Bacterial growth and lysis: me-tabolism and structure of the bacterial sacculus. Springer Science+Busi-ness Media, New York, NY.

59. Potluri L, Karczmarek A, Verheul J, Piette A, Wilkin J-M, Werth N, Banzhaf M, Vollmer W, Young KD, Nguyen-Distèche M, den Blaauwen T. 2010. Septal and lateral wall localization of PBP5, the major D,D-carboxypeptidase of Escherichia coli, requires substrate recognition and membrane attachment. Mol Microbiol 77:300–323. https://doi.org/10.1111/j.1365-2958.2010.07205.x.

60. Kohlrausch U, Höltje JV. 1991. Analysis of murein and murein precursors during antibiotic-induced lysis of Escherichia coli. J Bacteriol 173:3425–3431. https://doi.org/10.1128/jb.173.11.3425-3431.1991.

61. Templin MF, Ursinus A, Höltje JV. 1999. A defect in cell wall recycling triggers autolysis during the stationary growth phase of Escherichia coli. EMBO J 18:4108–4117. https://doi.org/10.1093/emboj/18.15.4108.

62. Cheng Q, Park JT. 2002. Substrate specificity of the AmpG permease required for recycling of cell wall anhydro-muropeptides. J Bacteriol 184:6434–6436. https://doi.org/10.1128/JB.184.23.6434-6436.2002.

63. Vötsch W, Templin MF. 2000. Characterization of a beta-N-acetylglucosaminidase of Escherichia coli and elucidation of its role in muropeptide recycling and beta-lactamase induction. J Biol Chem 275:39032–39038. https://doi.org/10.1074/jbc.M004797200.

64. Höltje JV, Kopp U, Ursinus A, Wiedemann B. 1994. The negative regulator of beta-lactamase induction AmpD is a N-acetyl-anhydromuramyl-L-alanine amidase. FEMS Microbiol Lett 122:159–164. https://doi.org/10.1111/j.1574-6968.1994.tb07159.x.

65. Jacobs C, Joris B, Jamin M, Klarsov K, Van Beeumen J, Mengin-Lecreulx D, van Heijenoort J, Park JT, Normark S, Frère JM. 1995. AmpD, essential for both beta-lactamase regulation and cell wall recycling, is a novel cytosolic N-acetylmuramyl-L-alanine amidase. Mol Microbiol 15:553–559. https://doi.org/10.1111/j.1365-2958.1995.tb02268.x.

66. Mengin-Lecreulx D, van Heijenoort J, Park JT. 1996. Identification of the mpl gene encoding UDP-N-acetylmuramate:L-alanyl-gamma-D-glutamyl-meso-diaminopimelate ligase in Escherichia coli and its role in recycling of cell wall peptidoglycan. J Bacteriol 178:5347–5352. https://doi.org/10.1128/jb.178.18.5347-5352.1996.

67. Dai Y, Pinedo V, Tang AY, Cava F, Geisinger E. 2021. A new class of cell wall-recycling L,D-carboxypeptidase determines $\beta$-lactam susceptibility and morphogenesis in Acinetobacter baumannii. mBio 12:e02786-21. https://doi.org/10.1128/mBio.02786-21.

68. Simpson BW, Nieckarz M, Pinedo V, McLean AB, Cava F, Trent MS. 2021. Acinetobacter baumannii can survive with an outer membrane lacking lipooligosaccharide due to structural support from elongasome peptidoglycan synthesis. mBio 12:e03099-21. https://doi.org/10.1128/mBio.03099-21.

69. Powers MJ, Trent MS. 2018. Phospholipid retention in the absence of asymmetry strengthens the outer membrane permeability barrier to last-resort antibiotics. Proc Natl Acad Sci U S A 115:E8518–E8527. https://doi.org/10.1073/pnas.1806714115.

70. Magnet S, Bellais S, Dubost L, Fourgeaud M, Mainardi J-L, Petit-Frère S, Marie A, Mengin-Lecreulx D, Arthur M, Gutmann L. 2007. Identification of the L,D-transpeptidases responsible for attachment of the Braun lipoprotein to Escherichia coli peptidoglycan. J Bacteriol 189:3927–3931. https://doi.org/10.1128/JB.00084-07.

71. Schroeder U, Henrich B, Fink J, Plapp R. 1994. Peptidase D of Escherichia coli K-12, a metallopeptidase of low substrate specificity. FEMS Microbiol Lett 123:153–159. https://doi.org/10.1111/j.1574-6968.1994.tb07215.x.

72. Schmidt DM, Hubbard BK, Gerlt JA. 2001. Evolution of enzymatic activities in the enolase superfamily: functional assignment of unknown proteins in Bacillus subtilis and Escherichia coli as L-Ala-D/L-Glu epimerases. Biochemistry 40:15707–15715. https://doi.org/10.1021/bi011640x.

73. Uehara T, Park JT. 15 October 2008, posting date. Peptidoglycan recycling. EcoSal Plus 2015. https://doi.org/10.1128/ecosalplus.4.7.1.5.

74. Das D, Hervé M, Feuerhelm J, Farr CL, Chiu H-J, Elsliger M-A, Knuth MW, Klock HE, Miller MD, Godzik A, Lesley SA, Deacon AM, Mengin-Lecreulx D, Wilson IA. 2011. Structure and function of the first full-length murein peptide ligase (Mpl) cell wall recycling protein. PLoS One 6:e17624. https://doi.org/10.1371/journal.pone.0017624.

75. White RJ, Pasternak CA. 1967. The purification and properties of N-acetyl-glucosamine 6-phosphate deacetylase from Escherichia coli. Biochem J 105:121–125. https://doi.org/10.1042/bj1050121.

76. Uehara T, Suefuji K, Valbuena N, Meehan B, Donegan M, Park JT. 2005. Recycling of the anhydro-N-acetylmuramic acid derived from cell wall murein involves a two-step conversion to N-acetylglucosamine-phosphate. J Bacteriol 187:3643–3649. https://doi.org/10.1128/JB.187.11.3643-3649.2005.

77. Uehara T, Suefuji K, Jaeger T, Mayer C, Park JT. 2006. MurQ etherase is required by Escherichia coli in order to metabolize anhydro-N-acetylmuramic acid obtained either from the environment or from its own cell wall. J Bacteriol 188:1660–1662. https://doi.org/10.1128/JB.188.4.1660-1662.2006.

78. Irazoki O, Hernandez SB, Cava F. 2019. Peptidoglycan muropeptides: release, perception, and functions as signaling molecules. Front Microbiol 10:500. https://doi.org/10.3389/fmicb.2019.00500.

79. Schindelin J, Arganda-Carreras I, Frise E, Kaynig V, Longair M, Pietzsch T, Preibisch S, Rueden C, Saalfeld S, Schmid B, Tinevez J-Y, White DJ, Hartenstein V, Eliceiri K, Tomancak P, Cardona A. 2012. Fiji: an open-source platform for biological-image analysis. Nat Methods 9:676–682. https://doi.org/10.1038/nmeth.2019.

80. Ducret A, Quardokus EM, Brun YV. 2016. MicrobeJ, a tool for high throughput bacterial cell detection and quantitative analysis. Nat Microbiol 1:16077. https://doi.org/10.1038/nmicrobiol.2016.77.

81. Wang N, Ozer EA, Mandel MJ, Hauser AR. 2014. Genome-wide identification of Acinetobacter baumannii genes necessary for persistence in the lung. mBio 5:e01163-14. https://doi.org/10.1128/mBio.01163-14.

82. Marolda CL, Lahiry P, Vinés E, Saldías S, Valvano MA. 2006. Micromethods for the characterization of lipid A-core and O-antigen lipopolysaccharide. Methods Mol Biol 347:237–252. https://doi.org/10.1385/1-59745-167-3:237.

83. Kazi MI, Perry BW, Card DC, Schargel RD, Ali HB, Obuekwe VC, Sapkota M, Kang KN, Pellegrino MW, Greenberg DE, Castoe TA, Boll JM. 2020. Discovery and characterization of New Delhi metallo-$\beta$-lactamase-1 inhibitor peptides that potentiate meropenem-dependent killing of carbapenemase-producing Enterobacteriaceae. J Antimicrob Chemother 75:2843–2851. https://doi.org/10.1093/jac/dkaa242.

84. Glauner B, Höltje JV, Schwarz U. 1988. The composition of the murein of Escherichia coli. J Biol Chem 263:10088–10095. https://doi.org/10.1016/S0021-9258(19)81481-3.

85. Kang KN, Klein DR, Kazi MI, Guérin F, Cattoir V, Brodbelt JS, Boll JM. 2019. Colistin heteroresistance in *Enterobacter cloacae* is regulated by PhoPQ-dependent 4-amino-4-deoxy-L-arabinose addition to lipid A. Mol Microbiol 111:1604–1616. https://doi.org/10.1111/mmi.14240.